Ventilazione di un canyon urbano con riscaldamento delle pareti o con presenza di vegetazione

metals

MDPI

Review

On the Use of Green and Blue Laser Sources for Powder Bed Fusion: State of the Art Review for Additive Manufacturing of Copper and Its Alloys

Mankirat Singh Khandpur [1,*], Alberto Giubilini [1,2], Luca Iuliano [1,2] and Paolo Minetola [1,2]

[1] Department of Management and Production Engineering (DIGEP), Politecnico di Torino, Corso Duca degli Abruzzi 24, 10129 Torino, Italy; alberto.giubilini@polito.it (A.G.); luca.iuliano@polito.it (L.I.); paolo.minetola@polito.it (P.M.)
[2] Integrated Additive Manufacturing Centre (IAM@PoliTO), Politecnico di Torino, Corso Duca degli Abruzzi 24, 10129 Torino, Italy
* Correspondence: mankirat.khandpur@polito.it

Abstract: Additive manufacturing (AM) is a layerwise production process that creates three-dimensional objects according to a digital model. This technology has demonstrated to be a promising alternative to conventional manufacturing methods for various industrial sectors, such as aerospace, automotive, biomedical, and energy. AM offers several advantages, like design flexibility, material efficiency, functional integration, and rapid prototyping. As regards metal parts, conventional AM techniques using infrared laser sources face some limitations in processing high-reflectivity and high-conductivity materials or alloys, such as aluminum, copper, gold, and silver. These materials have low absorption of infrared radiation, which results in unstable and shallow melt pools, poor surface quality, and high porosity. To overcome these challenges, green and blue laser sources have been proposed for AM processes. This review provides an overview of the recent developments and applications of green and blue laser sources for powder bed fusion of copper and its alloys, focusing on the effects of process parameters on the melt pool dynamics, microstructure formation, and thermal and electrical properties of the fabricated parts. This review also presents the main applications of AM of copper and its alloys together with potential opportunities for future developments.

Keywords: additive manufacturing; powder bed fusion; green laser; blue laser; copper alloys; industrial applications

Citation: Khandpur, M.S.; Giubilini, A.; Iuliano, L.; Minetola, P. On the Use of Green and Blue Laser Sources for Powder Bed Fusion: State of the Art Review for Additive Manufacturing of Copper and Its Alloys. *Metals* **2024**, *14*, 1464. https://doi.org/10.3390/met14121464

Academic Editor: Liuwei Zheng

Received: 31 October 2024
Revised: 13 December 2024
Accepted: 17 December 2024
Published: 22 December 2024

1. Introduction

Initially developed for prototyping application and tooling [1], layerwise fabrication has transformed from rapid prototyping [2] to 3D printing [1,3] and Additive manufacturing (AM) [4]. With the advancement of techniques to add the material layer after layer in different ways from solid, liquid, or powder feedstock [5], AM has demonstrated successful fabrication of metal parts, which can be used for both research and development (R&D) activities as well as for the fabrication of end-usable products.

The international joint guidelines ASTM F3177-21 [6] and ISO 52900 [7] establish a framework for the classification of additive manufacturing (AM) processes into seven categories: powder bed fusion (PBF), material extrusion (MEX), material jetting (MJT), binder jetting (BJT), sheet lamination (SHL), vat photopolymerization (VPP), and directed energy deposition (DED).

Figure 1 presents a classification of common direct and indirect AM techniques for metals. Direct methods produce fully dense metal parts in a single process, requiring only finishing or heat treatments. They can be broadly classified into two types based on layer formation methods: PBF, where powder layers are selectively fused by an energy source, and DED, where material is delivered and fused at the point of energy application. Indirect

methods create an intermediary product that is transformed into a metal part through steps like debinding and sintering.

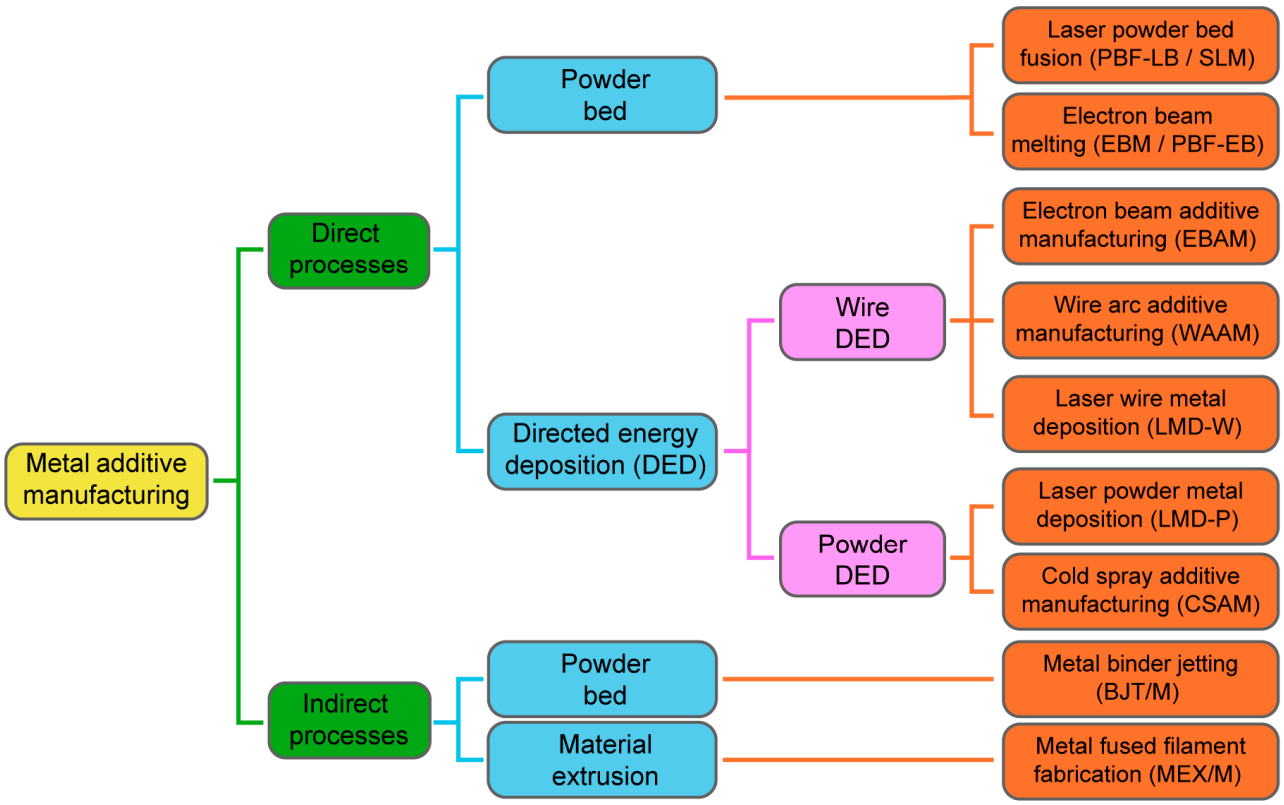

Figure 1. Classification of AM techniques for metals.

Laser-based AM encompasses several direct techniques, but Powder Bed Fusion–Laser Beam (PBF-LB) is the most important because of its diffusion and reliability for industrial applications [8]. PBF is recognized for its capacity to manufacture complex structures, such as internal channels, intricate support networks, and detailed surface features, that are challenging or impossible to create with traditional manufacturing techniques. This makes it an invaluable technique for industries requiring high-precision, custom parts with complex geometries. Previously published literature reported different industrial applications for laser-based AM technology, such as aerospace, sport racing, and the oil and gas industry [9]. Figure 2 represents the growth of industrial and academic interest in AM by plotting the growth of number of citations over the last 30 years. However, the data from recent years, starting from 2018, may not accurately reflect trends, as citations for recent publications are typically lower in number. The data were extracted from SciVal benchmark metrics [10] in August 2024 using different groups of keywords as detailed hereafter:

- Additive Manufacturing; Aluminum Alloys; Three Dimensional Printing—topic T.5515;
- Additive Manufacturing; Selective Laser Melting; Three Dimensional Printing—topic T.210;
- Additive Manufacturing; Titanium Alloys; Crystal Structure—topic T.3465;
- Copper Alloys; Selective Laser Melting; Three Dimensional Printing—topic T.86558;
- Additive Manufacturing; Copper Alloys; Three Dimensional Printing—topic T.84520.

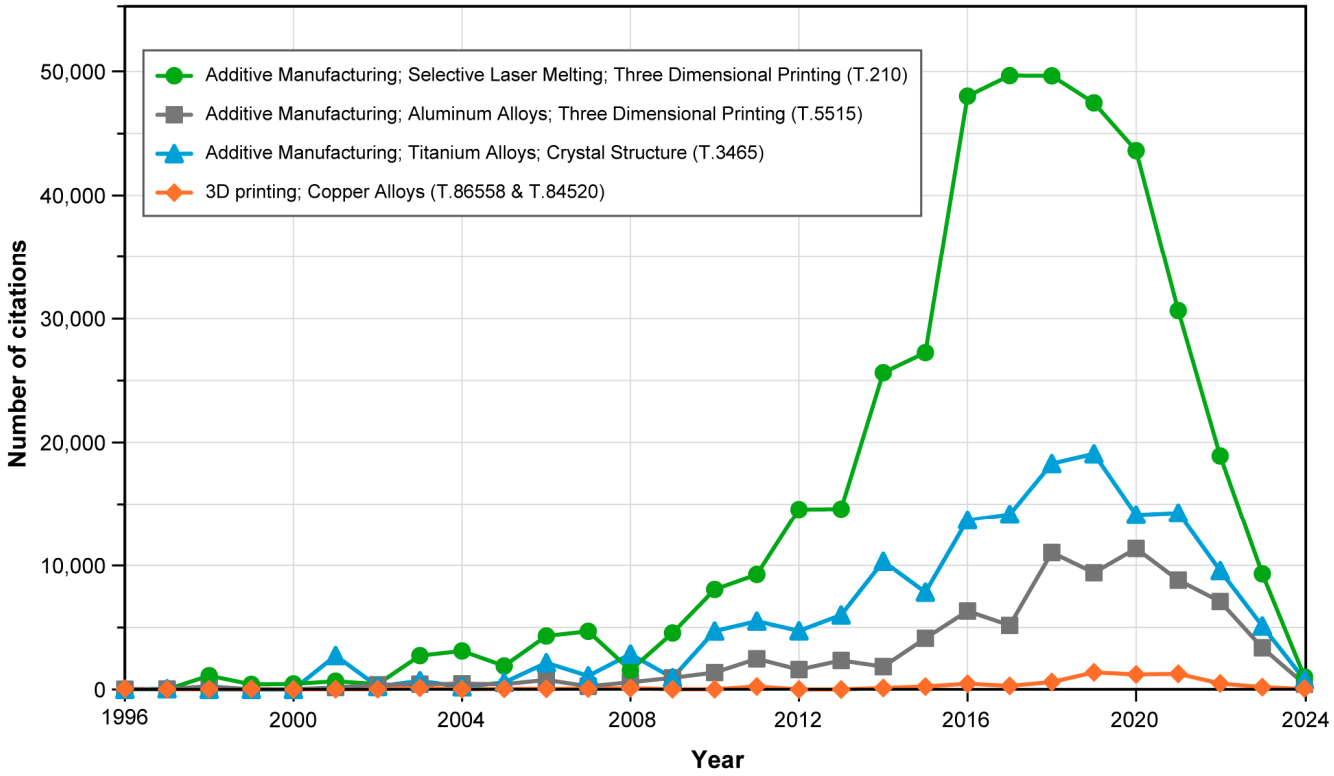

Figure 2. Growth of citation counts over the years for Additive Manufacturing from SciVal benchmark metrics.

The number of citations of the last two topics are grouped for the representation of the historical trend in Figure 2. The lowest number of citations for copper alloys on the one hand derives from the limited range of applications with respect to other metals like steel or aluminum. On the other hand, copper has demonstrated low processability by PBF-LB using conventional infrared sources.

This review aims to outline advancements in innovative laser sources used in PBF-LB, with a comprehensive examination of green and blue lasers for highly reflective metals with a specific focus on copper and its alloys. We aim to compare these sources with the common infrared laser used in PBF-LB, exploring the fundamental principles, recent advancements, challenges, and future trends associated with this AM technology. This paper begins with an introduction to the PBF-LF process and its core principles, including laser-material interaction. Subsequently, the paper delves into the use of innovative green or blue laser sources, with two dedicated sections detailing their advancements for application in AM. A separate section discusses the process parameters and optimization strategies for these innovative sources in PBF-LB. The following part of the review addresses the microstructure and functional properties of the produced parts or specimens, as presented in the literature by various authors. This is followed by a section on industrial applications, offering a broad perspective on the areas where the PBF process with innovative lasers for copper alloys is being adopted or is promising for the development of AM. Finally, the paper concludes with a discussion of current challenges in this field.

2. Fundamentals of Laser Powder Bed Fusion Technology

2.1. Process Description

PBF-LB builds parts incrementally, layer by layer, through the precise application of heat from a thermal laser source that locally melts a bed of fine metal powder into a fully formed solid object (Figure 3).

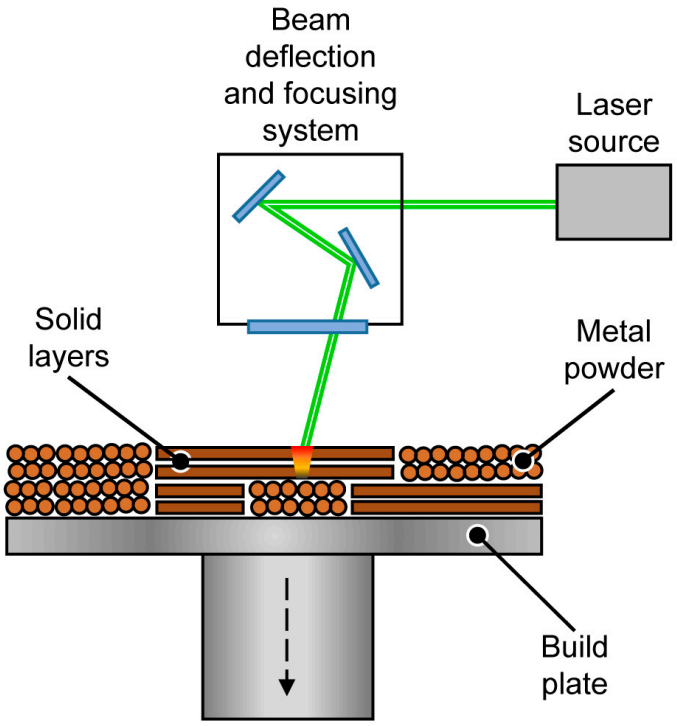

Figure 3. Scheme of the PBF-LB process with a green laser source for copper powder.

After loading of the feedstock powder in the machine, a thin layer of the metal powder, ranging from 20 to 100 microns, is spread across the build platform by a recoating blade or roller. As the laser passes over the powdered surface, it selectively melts the metal particles, effectively fusing them together in the designated areas of the CAD model, where the cross-section of the 3D object should be solid. After each layer is complete, the build platform lowers by the height of the layer, and a new layer of powder is evenly spread. This cycle repeats, with the laser fusing each successive layer of powder until the entire part is constructed. After the final layer is fused, the build chamber cools for several hours, depending on the part's size and complexity. The part is then removed, cleaned of loose powder, and often requires post-processing. This may include heat treatments to relieve stresses, support removal, surface finishing, or additional machining for precision. Compared to PBF-EB and Laser Powder Directed Energy Deposition (LP-DED), PBF-LB offers superior precision and smoother final surfaces. However, its reliance on laser-absorbing materials can limit energy absorption and process efficiency. In contrast, PBF-EB is better suited for conductive materials and offers faster build rates but lacks the fine resolution of PBF-LB and is limited by vacuum requirements [11]. LP-DED enables the production of larger parts with high deposition rates and no need for support structures, but it sacrifices resolution and surface finish quality compared to both PBF techniques. [12].

2.2. Laser-Material Interaction

In PBF-LB, it is essential to have precise control over laser parameters, powder characteristics, and environmental conditions to fabricate parts with the desired shape, size, strength, and appearance. The choice of laser type is largely determined by its interaction with the material, which is influenced by the material's absorption characteristics, laser power, beam size, and material phase.

The absorption coefficient of a material, indicating how much laser energy is absorbed per unit depth, is critical. This coefficient is strictly dependent on the laser wavelength and the material's surface condition. Typically, shorter wavelengths, such as ultraviolet or visible light, have higher absorption coefficients than longer wavelengths like infrared, as they interact more strongly with material electrons. However, some materials exhibit

specific absorption peaks or valleys at certain wavelengths due to their atomic or molecular structures. For example, copper and its alloys show significant variation in absorption with wavelength. Figure 4 shows the absorption coefficient of some processable metals in the solid state as a function of wavelength.

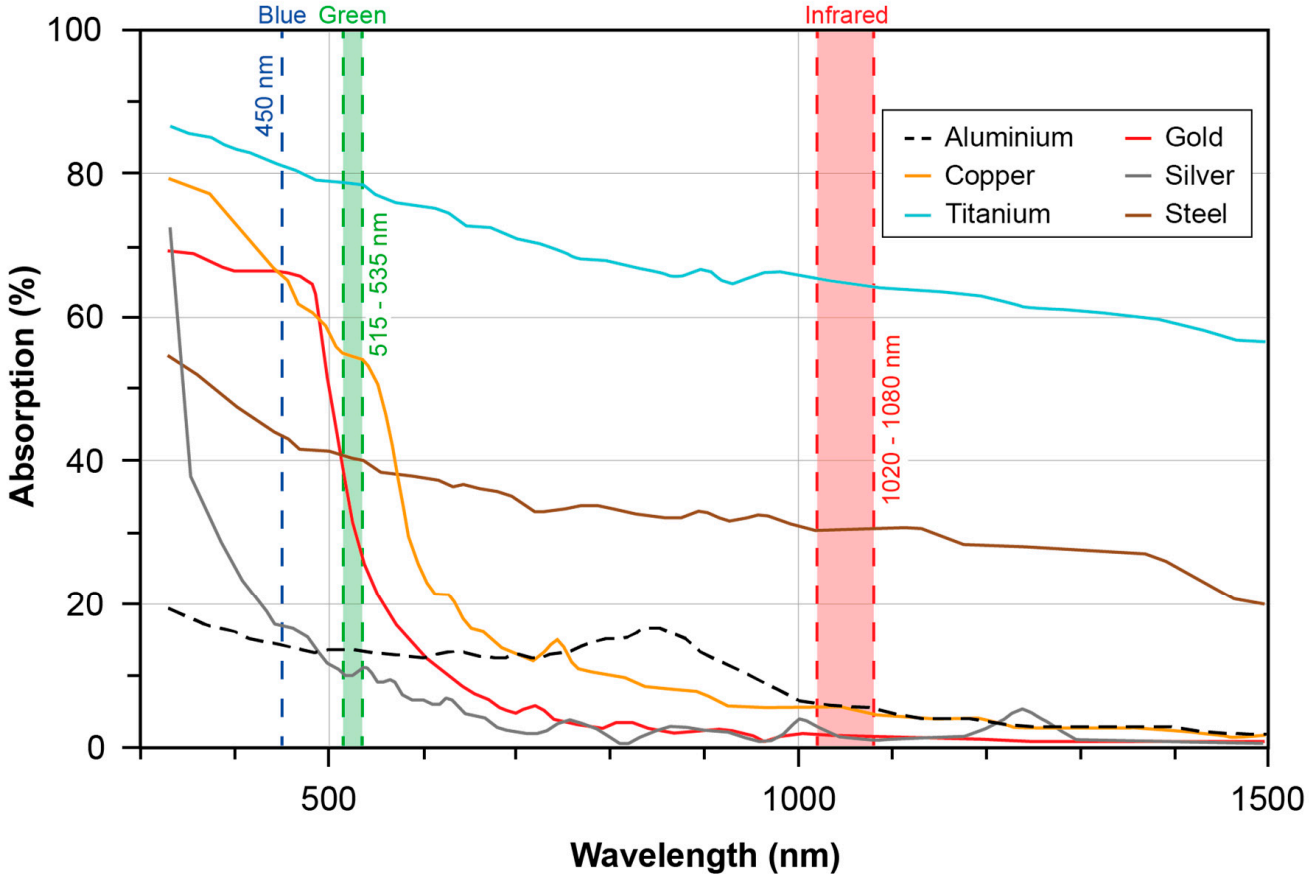

Figure 4. Absorption vs. wavelength for different solid materials. Adapted from Ref. [13].

In the near-infrared region, which is commonly used for PBF-LB, laser cutting, and welding, solid copper has a low absorption coefficient, leading to most of the laser energy being reflected. This necessitates high laser power and prolonged irradiation times to achieve adequate heating and melting, which can result in a large heat-affected zone (HAZ) and potential thermal damage or distortion. This issue is highlighted by simulations that show that inadequate heat dissipation during multilayer printing can lead to defects like cracks [14]. Conversely, in the visible light wavelength range, where solid copper has a high absorption coefficient, the material absorbs most of the laser energy, allowing for rapid heating and melting with lower laser power and shorter irradiation times. This results in a smaller HAZ, reducing thermal damage and distortion. However, high absorption in this range can lead to excessive vaporization and ablation rather than melting and bonding, requiring careful control of process parameters to avoid excessive material removal.

The interaction of the laser beam with material powder in laser bed fusion involves complex physical and chemical phenomena, such as melting, solidification, evaporation, ablation, oxidation, and spatter. These interactions affect the final product's density, porosity, surface roughness, and mechanical strength. For example, A. Singh et al. demonstrated that optimizing beam diameters can improve material density and reduce issues related to powder ejection [15]. Understanding these factors and their interplay is crucial for optimizing laser processing and achieving high-quality results in AM. Additionally, Nordet et al. explored the interaction between the laser, the underlying solid layer, and the powders. Material phase plays a key role in absorption, as demonstrated by a previous study that

quantified energy absorption variations for different phases. For example, copper absorbs approximately 75% of energy in its solid phase, 50% in the liquid phase, and 80–90% in keyhole regime [16]. Another study reported that copper powder absorbs more thermal energy from the laser compared to the underlying solid layer [17]. This is due to the poor thermal conductivity of the powder, which retains more heat than the solid layers, while the solid layers can effectively conduct the heat away, creating a thermal gradient. This gradient results in different melt pool conditions for solid layers versus powder layers. Horn et al. discussed that excess energy trapped in the powder can result in a laser polishing effect on previously solidified layers [18].

The quality of parts produced by PBF-LB is significantly influenced by the particle size of the metal powder, with optimal results typically achieved when the particle size ranges between 10 µm and 60 µm. Variations outside this range can affect the packing density, flowability, and energy absorption during the laser melting process, potentially leading to defects such as porosity, poor surface finish, or incomplete melting [19]. Smaller particles often lead to higher packing density, lower porosity, and smoother surface finish. However, they also require more energy to melt and may result in increased spattering and evaporation. Conversely, larger particles can decrease energy consumption and thermal stress but may introduce more voids, irregularities, and defects in the part. Optimizing particle size distribution is therefore crucial to achieving an optimal balance between quality and efficiency for each material and process.

Gruber et al. demonstrate how different types of copper—oxygen-free pure copper (Cu-OF) and oxygenated electrolytic tough pitch copper (Cu-ETP)—exhibit varying behaviors concerning absorption, porosity, and mechanical properties [20].

Another critical factor is the preheating and post-treatment of the powder and the part. Preheating the powder can reduce the thermal gradient and residual stresses while improving powder flowability and density. However, it may also lead to oxidation, contamination, or phase transformations that can negatively affect the mechanical and chemical properties of the final part. Wagenblast et al. reported that recycled powder exposed to oxygen or humidity up to an acceptable level did not adversely affect part performance [21]. Furthermore, the components and levels of contamination in an alloy impact its melting behavior, heat transfer, and resistance to deformation.

Previous research has explored various strategies to enhance the processability of copper and its alloys in PBF-LB, aiming to increase optical absorption and reduce the final component porosity. Among these, surface modification of copper powders has garnered significant attention. Different examples of metal-coated powders were investigated. For example, thin metallic tin coatings can boost optical absorption by almost 170%, but sulfur-free powders are essential to prevent cracking and porosity [22]. Similarly, Ni-coated Cu powders optimize laser reflectivity and produce near-dense copper parts when using 0.4 wt% Ni content [23]. Notably, a complete surface alloying state consistently outperforms simple surface adhesion, as demonstrated by Nickel [23] and Carbon [24]. Carburized CuCr1 powder prepared by heat-treating a carbon-mixed CuCr1 alloy at 750 °C increases optical absorption and flowability, allowing the production of fully dense copper parts. In contrast, carbon-mixed powders suffer from nanoparticle detachment and poor wettability with liquid copper. Moreover, in CuNiSi alloys, minimizing oxygen content and avoiding elements such as Zn and Mg significantly lowered porosity [25].

When a copper alloy is melted by a laser, impurities within the alloy can negatively affect the fusion process. Impurities may lower the alloy's melting temperature, making it more fluid and prone to spattering and splashing. This can cause voids or holes in the solidified layer. Additionally, impurities can segregate during solidification, forming clusters or inclusions that weaken the alloy's mechanical strength and reduce its conductivity. These inclusions act as stress concentrators, potentially initiating cracks in the material, and, most importantly, they hinder its electrical and thermal conductivity. Therefore, impurities can lead to defects such as porosity or cracks in the laser-melted alloy.

The interaction time of a quasi-continuous wave (QCW) laser depends on the pulse duration and repetition frequency. Consequently, with QCW laser, the copper alloy is heated gradually during interaction. The temperature rise is not constant, as heat conductivity and absorption of the copper alloy vary with each exposure step. As the temperature increases, the heating rate accelerates due to higher absorptivity and lower heat conductivity at elevated temperatures [26].

Copper's high thermal conductivity and low laser absorption make it particularly susceptible to keyhole-related defects during PBF-LB. As already established in previous literature, keyholes form when the laser's intensity causes rapid vaporization of the metal, creating a deep cavity in the melt pool [16,26]. This instability can lead to porosity and cracking. At higher scanning speeds, reflections are minimized as energy exits the melt pool with reduced interaction, stabilizing the process and mitigating keyhole-induced defects (Figure 5a). In contrast, slower scanning speeds or higher laser power deepen the melt pool and increase random reflections at the vapor-liquid interface, increasing porosity and cracking issues (Figure 5b).

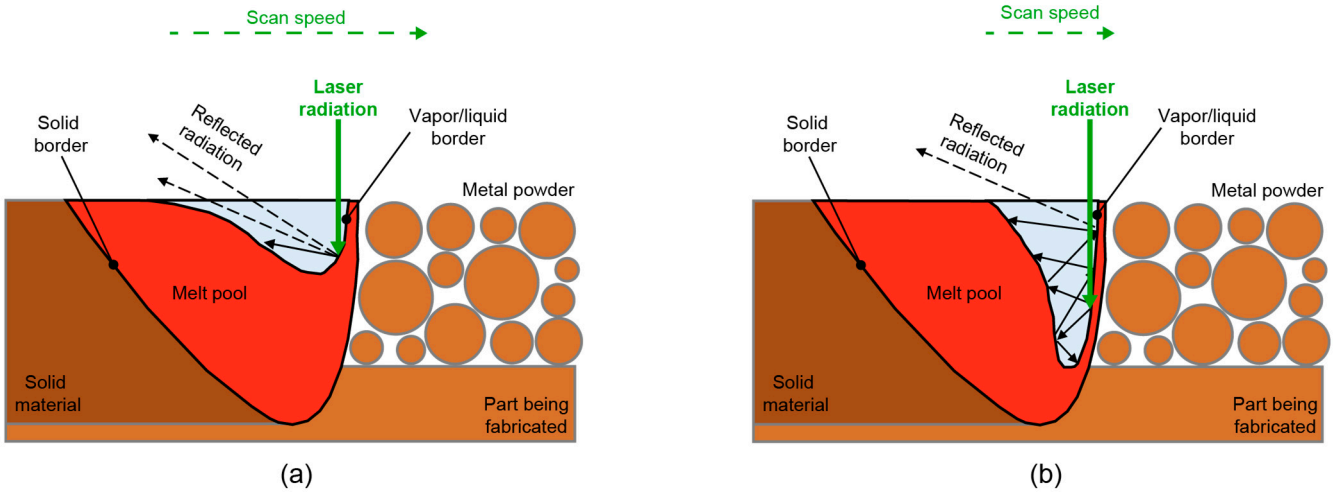

Figure 5. Representation of laser-powder for different scanning speeds: (**a**) high speed; (**b**) low speed.

In addition, the use of inert gas flows plays an important role in dissipating the heat generated by the laser during the melting process. These flows help conduct heat away from the build area, reducing the risk of overheating and minimizing thermal distortion in the workpiece. This temperature control is essential for producing high-quality parts with the correct microstructure and mechanical properties. Inert gases also contribute to maintaining the integrity of the metal powder that is not fused in the process. Because the powder is exposed to a low-oxygen environment, it is less prone to degradation and can often be reused for multiple builds, reducing material waste and cost.

2.3. Key Factors and Main Part Defects in PBF-LB

The PBF-LB process necessitates meticulous monitoring and control to ensure the quality and accuracy of the final product. The effectiveness of laser processing is greatly influenced by the properties of the material being used. Key factors influencing this process can be categorized into four main areas: properties of the feedstock material, laser source parameters, laser scanning strategy, and machine environment (Figure 6). In Sefene et al., the authors discuss the influence of process parameters on part quality [27].

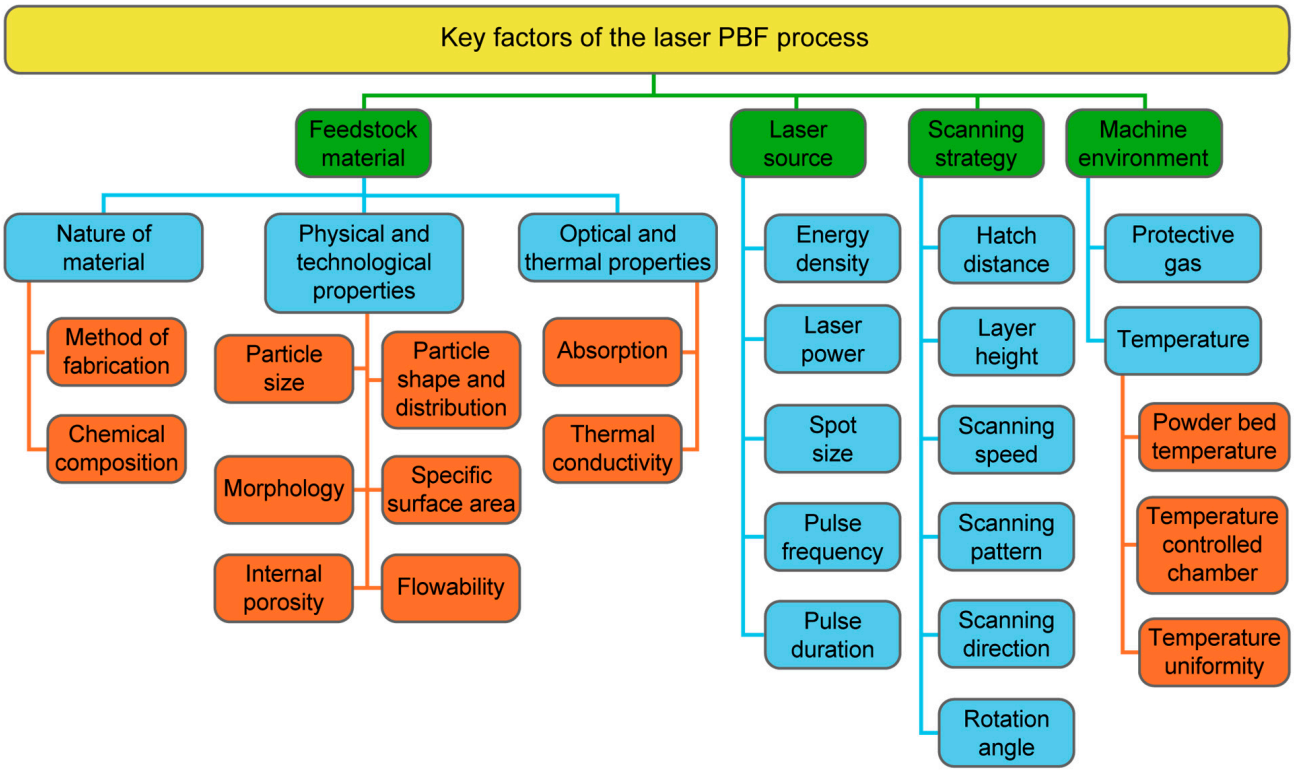

Figure 6. Classification of the key factors of the PBF-LB process. Adapted with permission from ref. [27]. 2024 Elsevier.

In PBF-LB, laser energy density is a critical parameter that defines the amount of energy delivered to the powder bed per unit area or volume. If energy density is too high, it can lead to material vaporization or defects like keyholing (deep, narrow melt pools), while energy density that is too low can cause incomplete melting or poor part cohesion. Equation (1) represents the volumetric energy density as a function of laser power P, scanning speed v, hatching distance h, and layer thickness t [28].

$$VED = \frac{P}{v \times h \times t} \quad (1)$$

Modifying energy density is essential for process optimization in PBF-LB. The right balance of energy density ensures that the powder particles are fully melted, guaranteeing minimal porosity, high dimensional accuracy, and mechanical performance.

Ongoing research continues to focus on refining laser architectures and optimizing process parameters to achieve properties comparable to traditional manufacturing methods [29]. In addition, processing highly reflective materials like copper with PBF-LB introduces new challenges. These challenges include the following:

- High reflectivity: Copper has a high reflectivity at the near-infrared (IR) laser wavelengths commonly used in PBF-LB, reflecting 90–98% of the incoming thermal energy and reducing process efficiency [29,30];
- High thermal conductivity: Copper's high thermal conductivity leads to rapid dissipation of heat from the melt pool, hindering the full re-melting of previously deposited copper [29,31];
- Porosity issues: Achieving high density in copper parts is challenging due to porosity issues, which affect the material's electrical resistivity [29,32];
- Different absorption rate: Copper has different absorption rates in its various phases (powdery, melt, solid) [28];

- Unstable melt pool: The melt pool can be unstable, resulting in balling and keyhole effects [29,33].

3. Innovative Types of Lasers in Powder Bed Fusion

IR lasers have been extensively developed and optimized over the years for a range of industrial applications, including welding, cutting, and marking. This maturity translates into a wealth of operational data, established processing parameters, and reliability. IR lasers, such as fiber lasers and Nd lasers, are widely available and generally less expensive than their blue or green counterparts. This cost-effectiveness, combined with their robustness and maintenance advantages, makes IR lasers a preferred choice in industrial settings where long operational lifetimes and low downtime are crucial. IR lasers, typically emitting at wavelengths around 1064 nm, are highly compatible with a wide range of metals and alloys used in industrial applications, including steels, titanium, and nickel-based superalloys. This broad compatibility simplifies the setup and tuning of the manufacturing process for different materials.

Nevertheless, as already mentioned, to overcome limitations and issues related to the processing of copper and its alloys in PBF-LB, innovative types of laser sources have been proposed as an alternative to IR lasers. The new sources use green or blue lasers, which typically operate at shorter wavelengths (e.g., 515 nm for green and 450 nm for blue), offering advantages in terms of reduced spot sizes and potentially higher resolutions. However, their current cost factors make them less ideal for widespread industrial use in metal additive manufacturing.

3.1. Advancements in Green Laser Technology

One of the main challenges in metal AM is to avoid thermal distortion and cracking caused by the high temperature gradients and residual stresses induced by the laser beam. Conventional infrared lasers have a low absorption rate for metals, with solid copper having an absorptivity of approximately 5% and liquid copper around 7%. This low absorptivity leads to inefficient energy transfer and excessive heat generation, adversely affecting process stability and part quality. In contrast, green lasers offer significantly higher absorption rates, improving energy efficiency and reducing thermal effects. For green lasers, the absorptivity of solid copper is expected to be comprised between 40% [34] and 60% [35], while that of liquid copper to be between 25% and 50% [16]. Interestingly, in the green wavelength region, solid copper absorbs more energy than liquid copper, a behavior opposite to that observed in IR lasers. This phenomenon may be attributed to interband transitions from the d-bands to the p-states at the Fermi level, which diminish in liquid copper, since temperature-induced band broadening occurs [36]. Green lasers were first created in the 1960s by using frequency-doubling crystals to convert the output of an infrared laser into a visible green beam [37]. They have been useful for different applications, such as laser pointers, optical storage, holography, and biomedical imaging. Recently, green lasers gained attention for metal AM due to their unique advantage over conventional IR lasers. Their shorter wavelength, ranging between 515 and 535 nm, allows for higher energy and greater precision in beam focusing [38]. Additionally, they are better absorbed by highly reflective metals such as copper, gold, or silver, which exhibit poor absorption in the IR wavelength range. However, green lasers have some drawbacks, including lower stability, higher sensitivity to environmental factors, and higher cost. Therefore, they are not suitable for all metal AM applications but are ideal for specific cases requiring high precision, quality, and performance. Green lasers, typically used in quasi-continuous wave mode [26], pulse mode [39], or continuous wave mode [21], offer unique properties for AM.

3.2. Advancements in Blue Laser Technology

Compared to green lasers, blue lasers, with a wavelength of approximately 450 nm [40], offer distinct advantages. Their shorter wavelength leads to improved absorption in

metals like copper, gold, aluminum, and titanium. For example, solid copper exhibits an absorption of approximately 65% for blue lasers, while liquid copper absorbs around 60% [41]. Their smaller spot sizes contribute to higher resolution and accuracy, allowing for the creation of complex geometries and finer features. Additionally, blue lasers form a smaller heat-affected zone (HAZ) on the targeted area, reducing thermal stress and distortion, which helps maintain the mechanical properties and dimensional accuracy of the printed parts. These characteristics are particularly beneficial for metal AM, as they enable more precise processing and better-quality results. In addition, blue lasers have a lower reflectivity and scattering effect than green lasers, thus reducing the risk of laser damages.

Conversely, blue lasers are more expensive and less available than infrared or green lasers, which are more mature and widely used in AM. Blue lasers also have lower brightness and less focused beams [16]. Additionally, they face challenges in scaling up and integrating with existing metal AM platforms due to their relative novelty. Ralf Jedamzik et al. reports that using the optical instrument with a high-power blue laser can lead to significant degradation [40]. Currently, blue lasers in literature are mostly used in hybrid mode, coupled mostly with IR lasers to improve the quality [42]. Overall, while blue lasers are more expensive and less widely available than green or infrared lasers, they offer superior performance in niche applications requiring high precision and reliability, such as aerospace, medical, and electronics industries. However, for applications needing higher power, lower cost, or compatibility with existing systems, other laser types may be more suitable.

4. Processability of Copper and Its Alloys by Innovative Lasers in PBF-LB

Due to the still limited number of studies on the influence of process parameters in short-wavelength PBF-LB, it is essential to determine whether the relationship, already well-established for IR lasers, can also be considered valid for green and blue lasers. More broadly, understanding how process parameters critically impact material properties and the overall quality of final products remains crucial. Table 1 presents general relationships between process parameters and process outcomes as recognized in the existing literature of blue and green laser sources.

To provide a comprehensive understanding of PBF-LB optimization for copper components, the following sections delve deeper into key factors such as laser power, scanning speed, and hatching distance, which significantly affect porosity content, electrical conductivity, thermal conductivity, and microstructure in the PB-LB process for copper and its alloys. Additionally, a dedicated section explores the influence of heat treatments on the most desired properties of copper components, i.e., thermal and electrical conductivity. First, the best results from previous literature dealing with the processing of pure copper and its alloys with IR lasers are presented. This establishes a foundational reference point, enabling a more structured and comprehensive comparison with the outcomes achieved using green and blue lasers in subsequent discussions.

Table 1. Main relationship between process parameters and process outcomes. "↑" stands for "increasing, while "↓" stands for "decreasing"

Process Parameter	Effect	References
↑ Laser power	↑ Density ↑ Degrees of texture ↑ Grain columnarity ↑ Melt pool depth	[43,44]
↑ Scan overlap	↑ Density ↓ Degrees of texture ↓ Grain columnarity	[44]

Table 1. *Cont.*

Process Parameter	Effect	References
↑ Scan speed	↓ Density ↓ Melt pool width	[43]
↑ Hatching distance	↓ Density ↑ Absorbance ↑ Overlapping area between adjacent single tracks ↑ Stability of the melt pool ↓ Roughness of single track	[16,26,42,43]
↑ Build volume	↓ Density ↑ Degrees of texture ↑ Grain homogeneity	[44]

4.1. Copper and Copper Alloys Processed Using IR Laser Source

Previous studies have demonstrated the feasibility of processing copper using IR source in PBF-LB. However, the final relative densities typically range from 80% to 90% [28,45]. Higher densities, with porosity lower than 1%, were achieved using high power laser (1 kW) and moderate scanning speed (500 mm/s). Typical build rates range from 12.6 cm^3/h [29] to 21 cm^3/h [46]. The process window is narrow; excessive energy density leads to deep melt pools and keyhole defects, while insufficient energy results in incomplete melting [47]. Optimized parameters stabilize the melt pool, yielding conduction-controlled, semi-elliptical melt pool shapes with minimal porosity. The resulting microstructures often consist of columnar grains oriented along the build direction, with strong <100> or <110> textures [47]. For copper processed with IR PBF-LB, studies indicate an almost linear correlation between relative density and conductivity. Conductivity values range from approximately 40% IACS [45] to 50–60% IACS at 85% relative density [48], reaching up to 88% IACS at nearly full density [47,49]. However, the thermal conductivity of pure copper samples fabricated by PBF-LB using IR lasers remains below 150 W/mK [50,51].

Copper alloys, such as CuCrZr and CuCrNb, were also processed by IR lasers. Near-full densities for CuCrZr, approaching 100%, were achieved with a volumetric energy density of about 500 J/mm^3 [52]. Alloying elements remain largely in solid solution, preserving desired material properties. However, the thermal and electrical conductivities of copper alloys are typically lower than those of pure copper.

4.2. Porosity Content

It is interesting to compare the use of short-wavelength sources, such as green or blue lasers, with near-infrared lasers to highlight the advantages of this approach. Firstly, a green laser can generate conduction melting, which allows for a larger hatching distance, resulting in a smoother surface and reduced internal defects. Additionally, a larger melt pool can be created at lower volumetric energy density (VED) due to the higher absorptivity of copper at a short wavelength. Ongoing research aims to refine processing parameters to enhance the performance and cost-effectiveness of PBF-LB-manufactured copper components. The primary parameters investigated in previous literature include laser power, scanning speed, and hatching distance. Among these parameters, laser power is pivotal; typically, it ranges from 100 W to 1000 W. However, reduced operating windows of laser powers were found satisfactory with short-wavelength lasers, where a laser power of approximately 200–400 W is sufficient to melt and bond the powder particles effectively. This is particularly important as it prevents the use of excessively high powers, thus reducing energy consumption, preventing keyhole formation, and avoiding porosity and reduced mechanical integrity [53]. Scan speed is another essential parameter; with short-wavelength lasers, it can range between 300 and 1200 mm/s. Optimal scan speeds are often around 500–700 mm/s and need to be balanced with heat input to avoid incomplete melting or excessive heat accumulation. Hatching distance also impacts part density and surface finish. Common hatching distance ranges from 80 to 150 µm. A narrower hatching distance ensures better

overlap between tracks, reducing the probability of porosity but increasing build time. In conclusion, optimizing PBF-LB process parameters for copper manufacturing requires a delicate balance. Fine-tuning laser power, scan speed, and hatching distance can lead to superior mechanical properties, reduced defects, and efficient production processes. In Appendix A, Tables A1 and A2 summarize the different processing windows and main findings explored by previous studies focused on the PBF-LB processing of copper and its alloys using short-wavelength lasers. Parts of these results are also graphically presented in Figure 7.

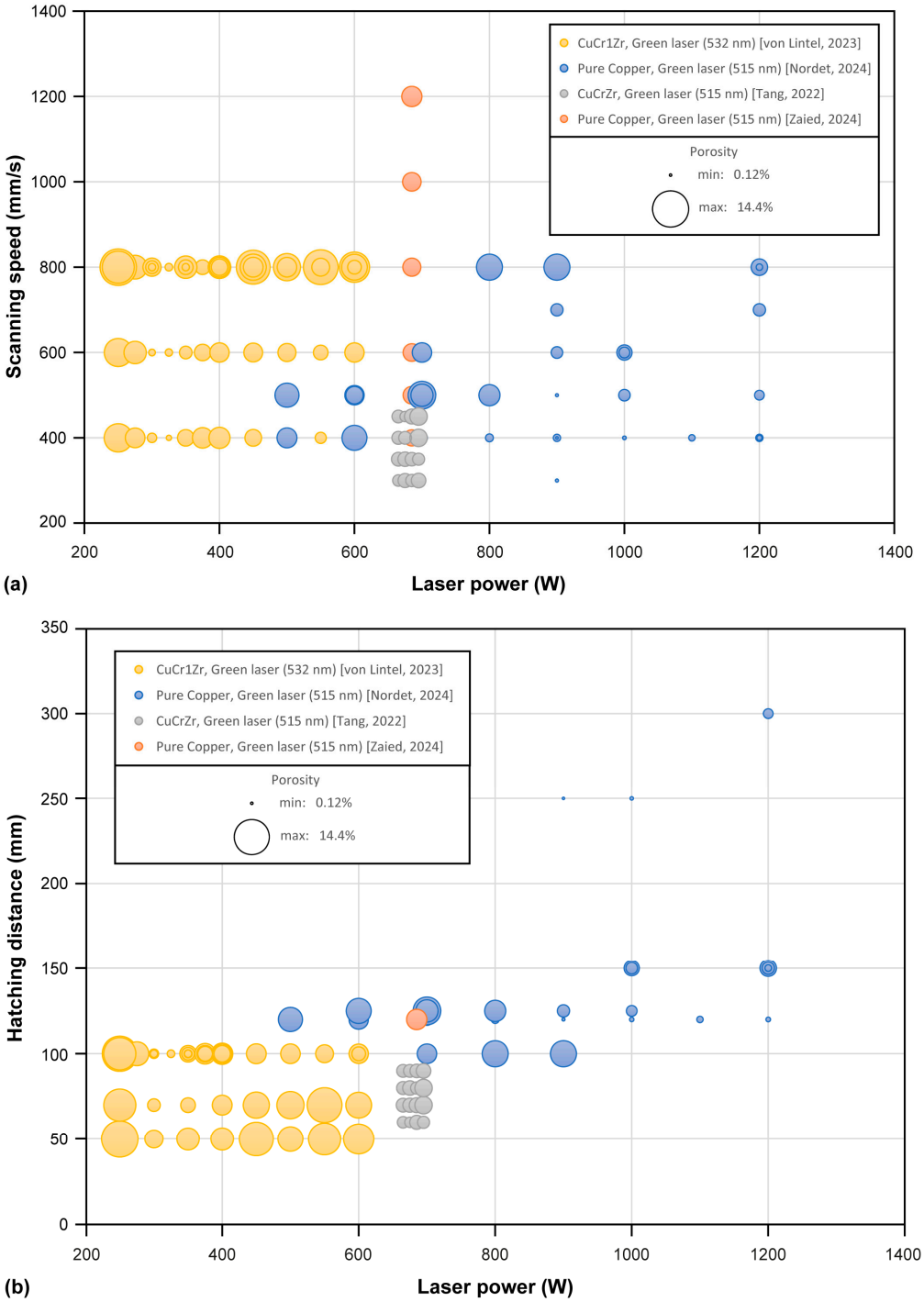

Figure 7. Porosity of PBF-LB copper and copper alloy samples reported from Refs. [26,46,54,55], shown as function of process parameters: scanning speed vs. laser power (**a**); hatching distance vs. laser power (**b**).

4.3. Electrical Conductivity

Copper is a highly requested material for electrical applications due to its excellent electrical conductivity, which is a result of its chemical structure, characterized by a single electron in its outermost orbital. Pure copper is one of the most conductive materials available nowadays, with a conductivity of 5.8×10^7 S/m at 20 °C, equivalent to 100% IACS (International annealed copper standard) [56]. In this regard, Figure 8 illustrates the results of previous studies that investigated the correlation between relative density and electrical conductivity for as-build copper and copper alloy components manufactured by green laser PBF-LB.

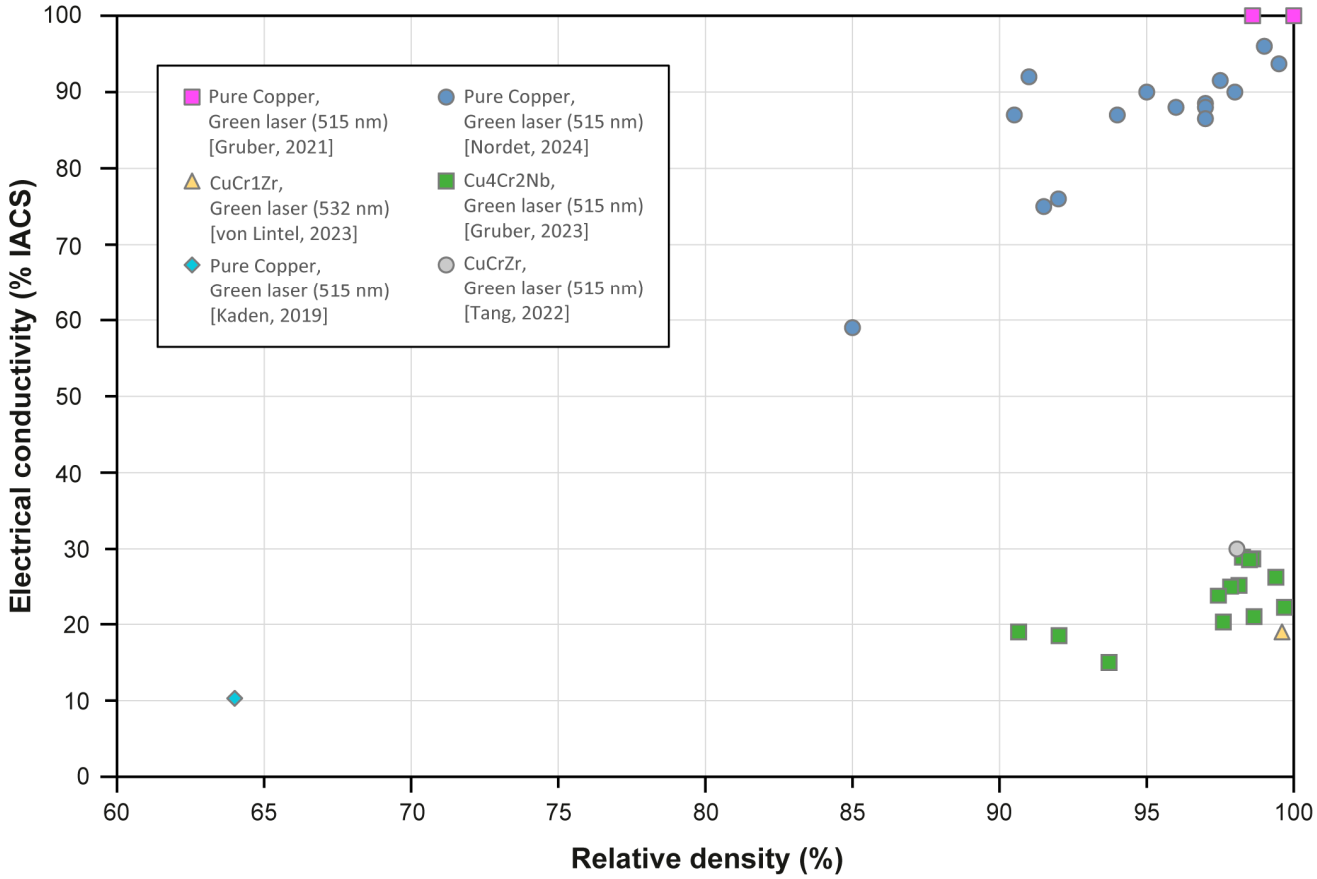

Figure 8. Electrical conductivity depending on the relative density of PBF-LB copper and copper alloy samples reported from Refs. [20,26,37,46,54,57].

Gruber et al. reported nearly 100% IACS for components produced with this technique, suggesting a promising approach for producing highly conductive components through AM. An almost linear increase in electrical conductivity with increasing relative density was observed [46,57], although absolute values varied. One primary factor for the decrease in electrical conductivity is the chemical composition of the feedstock material, as copper alloys possess much lower conductivity than pure copper [26,54]. Moreover, manufacturing conditions also significantly impact the final conductivity, with factors such as porosity, impurities, grain boundaries, and dislocations contributing to reduced electrical performance [58].

Another interesting aspect investigated by Gruber et al. is the impact of surface condition and wall thickness on electrical conductivity. Components with different surface finishes, such as sandblasted and milled, showed that milled surfaces always exhibited higher conductivity. This difference became more pronounced as wall thickness decreased, with a 0.5 mm wall having half the conductivity when sandblasted compared to milled [20].

4.4. Thermal Conductivity

A desirable property for copper components is thermal conductivity, which increases proportionally to electrical conductivity with respect to temperature, as described by Wiedemann–Franz's law (Equation (2)) [59]:

$$\lambda = L\sigma T \quad (2)$$

where, λ represents thermal conductivity, L denotes the Lorenz number (2.41×10^{-8} $\Omega W/K^2$), σ refers to electrical resistivity, which is the reciprocal of electrical conductivity, and T represents absolute temperature. Wrought copper exhibits a thermal conductivity of 398 W/mK at 30 °C [60]. However, achieving this value in as-built copper components produced by PBF-LB is challenging due to high-density dislocations, defects like unmelt powder particles, and high thermal stresses resulting from the rapid cooling rate. A significant limitation in thermal conductivity is the porosity of the sample. Pores or voids within a material create thermal barriers that hinder heat flow. Therefore, increased porosity typically reduces the material's thermal conductivity, resulting in lower heat transfer efficiency and poorer thermal performance. For example, Kaden et al. observed that thermal conductivity of pure copper samples processed by a green laser was an order of magnitude lower than the reference value for wrought copper, with a porosity of 36% [37]. Conversely, Zaied et al. achieved satisfactory thermal performance in components processed by green laser PBF-LB, with thermal conductivity values close to the copper reference, ranging from 362 to 392 W/mK, depending on internal porosity [55].

An interesting study by Xie et al. revealed thermal anisotropy in as-built samples processed by green laser PBF-LB. The thermal conductivity of CuCrZr alloys was slightly better along the transverse direction compared to the build direction [61]. Figure 9 illustrates previously published results for the thermal conductivity of copper and copper alloy components processed by green laser PBF-LB and measured as-built at room temperature.

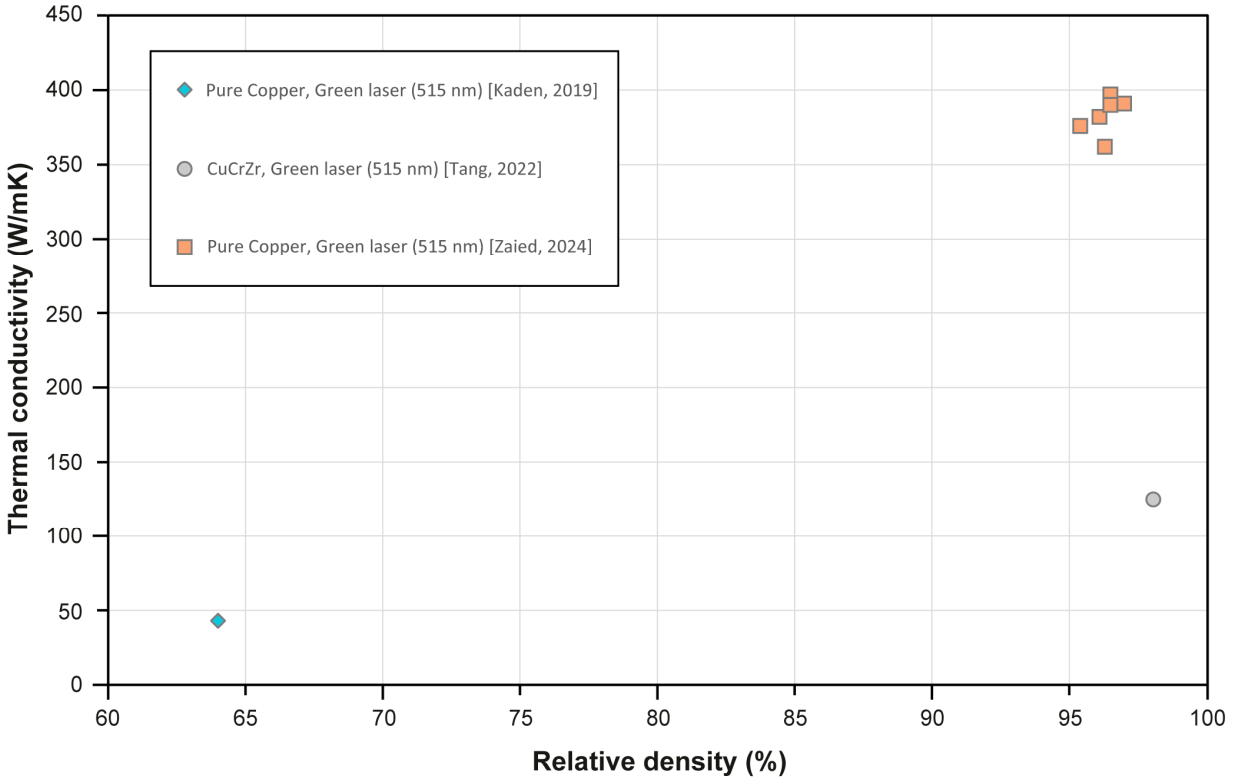

Figure 9. Thermal conductivity depending on the relative density of PBF-LB copper and copper alloy samples reported from Refs. [37,54,55].

4.5. Microstructure

The use of short-wavelength laser sources significantly enhances copper's energy absorption, resulting in higher energy density and more stable melt pool dynamics. This improvement is critical for achieving high-quality microstructures and enhancing processability and mechanical performance. Scanning electron microscopy (SEM) showed that copper parts produced by green laser PBF-LB typically exhibit a columnar microstructure oriented toward the build direction, with chevrons located at the center of large vertical columns (Figure 10a) [20,46,54]. The grain boundaries are clean, and no segregation of impurities was observed, indicating a more homogeneous solidification process. This homogeneity contributes to the overall mechanical strength and electrical conductivity of the copper parts. Notably, similar microstructural characteristics can be achieved using IR lasers when the appropriate energy density is applied, stabilizing the melt pool dynamics and forming a conduction-controlled semi-elliptical melt pool shape with minimal porosity, as shown in Figure 10b. However, achieving this requires precise parameter control, as the optimal energy density window is relatively narrow. Insufficient energy density can result in incomplete melting of copper, while excessive energy density can cause extremely deep melt pools, leading to keyhole pores and reduced density (Figure 10c). These findings highlight that both green and IR lasers can yield similar high-quality microstructures when carefully optimized, although IR lasers face greater challenges and generally require higher energy to overcome copper's low absorption efficiency.

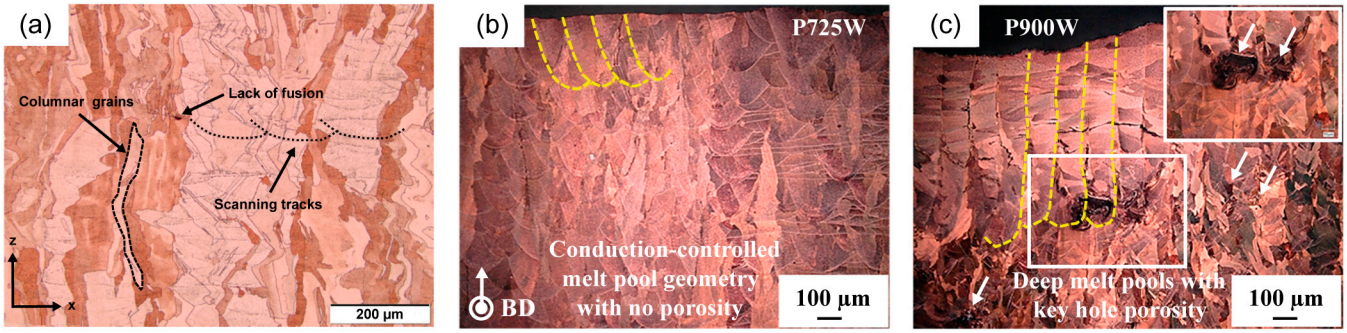

Figure 10. Microstructural characterization of pure copper manufactured by: (**a**) green laser with a linear energy density of 0.81 J/mm. Reprinted from Ref. [20]; (**b**) IR laser PBF with a linear energy density of 2.25 J/mm. Reprinted from Ref. [45]; (**c**) IR laser PBF with a linear energy density of 1.82 J/mm. Reprinted from Ref. [45]. Yellow dashed lines indicate melt pools, while white arrows highlight keyhole porosities.

When processing copper alloys instead of pure copper, previous studies on CuCrZr revealed that the concentrations of Cr and Zr remain comparable to those in the original powder, suggesting both elements remain in solid solution within the matrix and no micro-precipitates were encountered [26,54]. Xie et al. investigated the effect of aging treatment on this alloy and found that after aging, Cr precipitated uniformly as nano-scaled particles along both transverse and build directions [61]. Other copper alloys were also investigated, and the resulting microstructure strongly depended on the alloy composition. For example, Gruber et al. processed a Cu4Cr2Nb alloy, finding agglomerated round (20 µm) and elongated (40 µm) particles in the final component. These agglomerates exhibited a dendritic structure resulting from the direct precipitation of CrNb within the melt and the local concentration and agglomeration of the eutectic CrNb phase with high Nb content [58].

Crystallographic texture analysis, conducted using electron back-scattered diffraction (EBSD) mapping, is a key microstructural aspect in understanding the behavior of metals processed by PBF-LB. Typically, metals processed by PBF-LB exhibit a strong crystallographic texture along the building direction, as grains grow parallel to the temperature gradient, with <100> and <110> textures commonly observed in copper bulk compo-

nents [47,62]. However, in lattice structures, unmelted or partially melted particles serve as nucleation sites for new grains, which impedes texture development along the building direction [63]. As shown in Figure 11, the crystallographic texture of copper lattice structures manufactured with a green laser does not exhibit a strong directional preference, as evident from the pole figure maps. The EBSD map highlights two distinct regions, Area 1 (truss) and Area 2 (node), which show different crystallographic orientations. In Area 1, the truss regions, the <100> orientation is dominant, indicating a stronger alignment along the build direction, a result of the thermal gradients during the PBF-LB process. Conversely, Area 2, corresponding to the node regions, exhibits a more heterogeneous crystallographic texture, with a mix of <100>, <111>, and <110> orientations. This variation in texture is attributed to local differences in cooling rates and the geometry of the lattice, which influences grain growth and orientation. The pole figures for the <100>, <111>, and <110> crystallographic planes further confirm that the <100> orientation is more pronounced in the truss regions compared to the node areas.

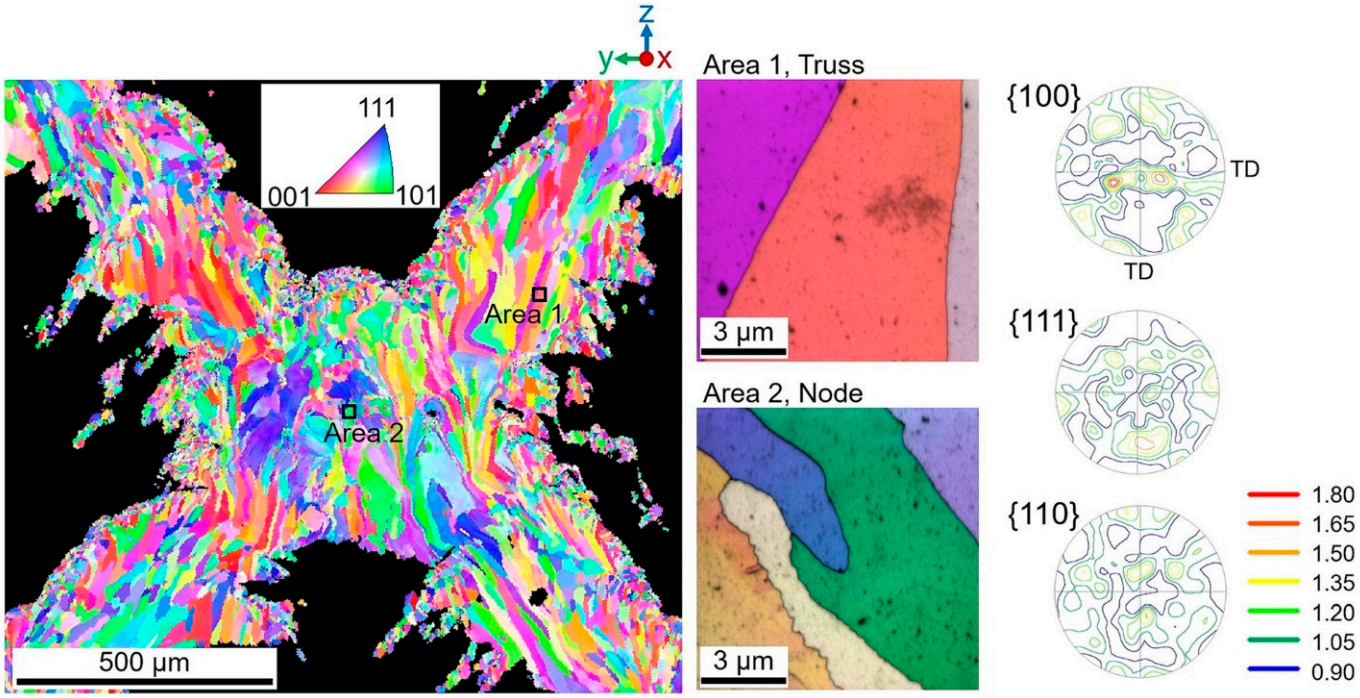

Figure 11. Crystallographic texture along the build direction of a pure copper lattice structure manufactured by green laser PBF. Reprinted from Ref. [64].

4.6. Heat Treatments

Similarly to their role in IR-laser processing, heat treatments play a significant role in enhancing the electrical and thermal properties of copper and copper-alloy components processed by PBF-LB with green lasers. Various studies explored the effects of different temperatures, durations, and methods, revealing their impact on electrical and thermal conductivity. Aging treatments were shown to improve electrical conductivity, with post-treated samples achieving up to four times the conductivity of as-built components [26,61]. This improvement is mainly due to the release of thermal stress and reduction in dislocation density, as well as the dissolution or rearrangement of precipitates in copper alloys.

The effect of heat treatment parameters has been extensively studied. Gruber et al. conducted a significant study on the effects of annealing temperatures and durations on the electrical conductivity of copper and copper alloys. Their findings demonstrated that annealing temperature had a predominant effect compared to time. For example, increasing the annealing temperature from 400 °C to 1000 °C doubled the electrical conductivity after a 30 min treatment. Conversely, extending the treatment duration from 30 min to 4 h at the same temperature had a minimal effect. The study also compared different treatments,

including hot isostatic pressing (HIP), and found that conventional annealing treatment at 500 °C was more effective for improving electrical conductivity [58].

Thermal conductivity enhancements through heat treatments were similarly explored. Previous research demonstrated that direct aging treatment at 500–550 °C significantly increased the thermal conductivity of copper and copper-alloy components, often tripling the as-built values. For instance, direct aging at 500 °C for 1 h increased thermal conductivity from approximately 110 W/mK to 305 W/mK in the transverse direction [61]. Tang et al. compared two different heat treatments, solution annealing, and direct aging hardening to determine the influence of time and temperature on thermal conductivity. They found that longer aging time or higher aging temperatures considerably improved the thermal properties of the copper alloy, mainly due to the temperature and time-dependent behavior of precipitates. Notably, the authors demonstrated that solution annealing at 960 °C for 1 h was less effective for enhancing thermal conductivity compared to direct aging at 550 °C for 1 h [54]. Table 2 consolidates the findings from multiple studies, summarizing the effects of different heat treatments on the electrical and thermal properties of copper and copper-alloy components processed by green laser PBF-LB.

Table 2. Effect of heat treatments on electrical and thermal conductivity of copper and copper-alloy components processed by green laser PBF. "N.D." stands for "not declared".

Material	Heat Treatment	Relative Density [%]	Electrical Conductivity [% IACS]	Thermal Conductivity [W/mK]	Ref.
Pure copper	Heat treatment at 200 °C for 1 h	98	94	N.D.	[46]
	Heat treatment at 200 °C for 1 h	99	93	N.D.	
	Heat treatment at 500 °C for 1 h	99.5	94.6	N.D.	
	Heat treatment at 200 °C for 1 h	97	87	N.D.	
	Heat treatment at 500 °C for 1 h	97.5	93	N.D.	
	Heat treatment at 500 °C for 1 h	97	87.2	N.D.	
	Heat treatment at 200 °C for 1 h	97	88	N.D.	
	Heat treatment at 500 °C for 1 h	94	86	N.D.	
Copper alloy (Cu4Cr2Nb)	Heat treatment at 400 °C for 30 min	N.D.	44	N.D.	[58]
	Heat treatment at 400 °C for 4 h	N.D.	50	N.D.	
	Heat treatment at 500 °C for 30 min	N.D.	69	N.D.	
	Heat treatment at 600 °C for 30 min	N.D.	80	N.D.	
	Heat treatment at 700 °C for 30 min	N.D.	84	N.D.	
	Heat treatment at 700 °C for 4 h	N.D.	84	N.D.	
	Heat treatment at 1000 °C for 30 min	N.D.	86	N.D.	
	Heat treatment at 1000 °C for 4 h	N.D.	86	N.D.	
Copper alloy (CuCrZr)	As-built	N.D.	N.D.	112	[61]
	Direct aging hardening at 500 °C for 1 h + cooling under N_2 atmosphere in furnace	N.D.	64	305	
Copper alloy (CuCrZr)	As-built	N.D.	N.D.	125	[54]
	Solution annealing at 960 °C for 1 h + water quenching	98.07	56	233	
	Solution annealing at 960 °C for 1 h + water quenching + aging hardening at 500 °C for 1 h	98.07	84	350	
	Direct aging hardening at 500 °C for 1 h	98.07	64	266	
	Direct aging hardening at 500 °C for 2 h	98.07	78	325	
	Direct aging hardening at 550 °C for 1 h	98.07	83	346	
Copper alloy (CuCr1Zr)	Annealing at 480 °C for 2 h	99.6	67.5	N.D.	[26]

5. Industrial Applications

Copper and its alloys are used in various high-performance industrial applications that require materials to endure harsh operating conditions while retaining outstanding electrical and thermal properties. These applications highlight the versatility of copper and its alloys in various industries, particularly where thermal and electrical conductivity are critical. Additive manufacturing plays a significant role in advancing these applications by enabling complex and optimized designs [65]. Innovative green and blue laser sources may also improve powder bed fusion efficiency in those applications where infrared sources or other types of AM processes have been proposed or used. The most common applications are presented and discussed hereafter.

5.1. Electric Motors and Generators

Copper is preferred for manufacturing electrical and electromagnetic devices due to its excellent conductivity. Pure copper windings and rotors play a crucial role in electric motor performance. Recently, in the automotive sector, the demand for copper has increased with the rise of hybrid and electric vehicles.

In their work, Szabó and Fodor extensively cover the potential applications and advancements of additive manufacturing (AM) in the field of electrical machines, particularly focusing on components such as windings, iron cores, and cooling systems [66]. AM technologies enable the creation of complex winding geometries that are not possible with traditional manufacturing methods. This includes the production of windings with precise configurations that can significantly enhance the performance of electrical machines by improving magnetic field distribution and reducing electrical losses.

AM delivers the flexibility of producing complex geometries and integrating multiple functions into single components, which traditional manufacturing cannot achieve. This capability is especially beneficial in creating densely packed, high-efficiency electrical machines (Figure 12a).

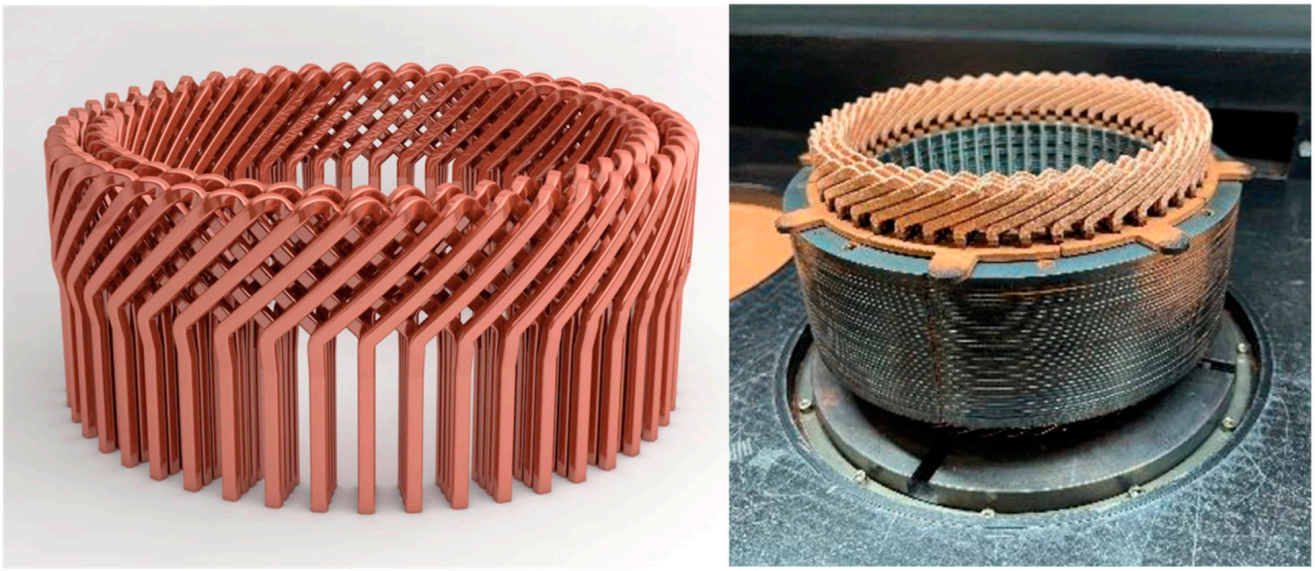

Figure 12. 3D-printed hairpin windings for electric motors (**a**), reprinted from Ref. [67]; 3D-printed hairpin head mounted on conventional stator windings (**b**), reprinted from Ref. [68].

Selema et al. emphasize the benefits of AM in achieving high material efficiency and reducing waste compared to conventional methods [67]. The study by Putz et al. explores the application of hybrid PBF-LB for manufacturing hairpin winding heads in electric traction drives, focusing on pure copper as the material of choice [68]. The authors investigate the feasibility of directly printing complex winding heads on conventional

copper conductors, aiming to integrate AM into the production of hairpin stators for electric traction drives (Figure 12b). This method allows for tool-free production and increased flexibility in design. By using PBF-LB, the research highlights potential reductions in the height of winding heads, which consequently decreases copper material usage and minimizes losses in electric machines, leading to increased efficiency. Concentrated coils with intricate shapes can be produced by AM with the aim of designing more efficient electromagnetic configurations.

Simpson et al. [69] explored innovative strategies in the manufacturing of electrical windings for high-power density and energy-efficient machines using AM for functionally graded materials. Their work discusses the potential to functionally grade materials within a winding to optimize the balance between DC and AC losses. This is achieved by manipulating the electrical conductivity at different sections of the winding through controlled porosity using the PBF-LB process. It was found that the electrical conductivity of CuCrZr alloy could be varied by adjusting the laser energy during the manufacturing process. This enables the production of windings with spatially varied properties that can potentially reduce overall energy losses in electrical machines.

Innovations in cooling systems for electrical machines are also explored, with a focus on using AM to create more efficient and compact cooling channels within windings and motor structures. This helps in managing the heat more effectively, thus improving the reliability and performance of the motors. Cooling channels can also be integrated within the copper windings (Figure 13a) for improvement of the heat dissipation in high-power electrical machines [48]. Rajan and Tangudu demonstrated that liquid-cooled windings fabricated by AM can tolerate a current density of 20 A/mm^2 [70].

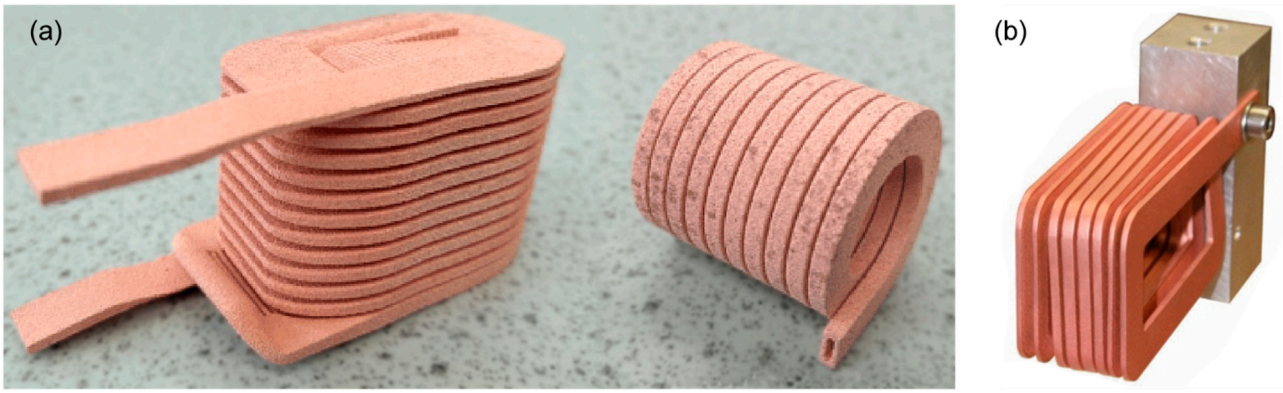

Figure 13. Concentrated PBF-LB hollow winding (**a**), reprinted with permission from Ref. [48]. 2024 Elsevier; mounting of concentrated copper alloy windings (**b**), adapted from Ref. [71].

Besides windings for electric motors, LPF-LB copper parts can also be employed in batteries for electromobility applications [72]. AM can enhance the electrode structure, notably through customized pore sizes that improve mass transfer and stability, resulting in higher power densities compared to traditional copper foam electrodes [73]. AM copper current collectors can be used to produce structural lithium-ion batteries, potentially enhancing the performance and structural integrity of batteries [74]. PBF-LB of copper and its alloys offers a sustainable and efficient alternative for directly manufacturing end-use parts, compared to other methods that rely on 3D printing of polymeric bases for subsequent copper layer deposition on the part surface.

Another aspect to be considered is the role of AM in enhancing the resilience and responsiveness of supply chains for electric battery production, particularly in scenarios where material procurement becomes challenging. Current supply chain structures for lithium-ion batteries (LIBs), which are crucial for electric and hybrid vehicles, are complex and not optimized, leading to high costs and environmental impacts. The work by Cagliano et al. [75] discusses the environmental impact of long-distance transportation of battery components and the potential benefits of local production. Integrating AM technology

for copper elements could enhance this framework by providing flexibility to produce battery components locally, reducing dependency on volatile supply chains. It can enable manufacturers to react swiftly to changes in material availability by adapting designs or materials used based on what is accessible. AM can contribute by allowing more localized manufacturing of battery parts, reducing transportation needs, and potentially lowering the carbon footprint of the production process.

5.2. Heat Inductors

Additive manufacturing has been used to produce inductors for intricate and localized tools for heat treatments like induction hardening. Induction hardening is utilized in the metal-processing industry, particularly among automotive suppliers, and in any scenario where specific component surfaces must endure significant mechanical stress and wear. This surface hardening technique focuses only on the outer layer of a component rather than the entire piece.

To perform induction hardening, a coil made of highly conductive copper tubes, through which high-pressure cooling water circulates (Figure 14a), surrounds the component. A high-frequency alternating current passes through this induction coil, creating an intense magnetic field. This magnetic field induces eddy currents in the component's surface layer, generating frictional heat that causes it to glow. As a result, the surface heats rapidly to the necessary temperature for hardening. The component is then quenched in water to complete the hardening process. The depth of the hardened surface layer can be adjusted; higher frequencies result in shallower hardening. After a predetermined duration, the heated surface is quenched. The combination of intense heating and rapid cooling enhances the component's strength. Additionally, the more closely the inductor's shape matches the component's contour, the more uniform the hardness distribution will be. Standard inductors may lose effectiveness during hardening compared to custom-designed ones tailored for specific applications. AM inductors provide dimensional repeatability, extended lifespans due to the elimination of braze joints, and lower fabrication costs. They are especially advantageous for high-volume heat treatment applications or those that require precise heat treatment patterns (Figure 14b). Additive manufacturing has been used to produce copper inductors for heat treatment tooling. These inductors offer dimensional repeatability and reduced fabrication costs, making them suitable for high-volume heat treatment applications.

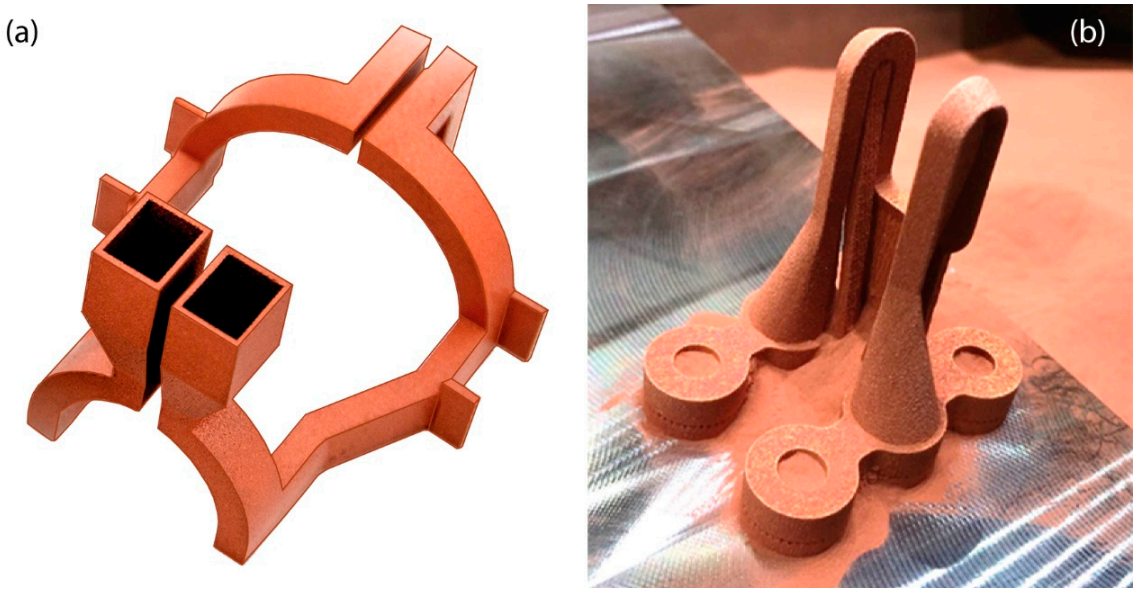

Figure 14. Induction coil with inner channels for liquid cooling (**a**); induction heater with integrated water cooling (**b**), reprinted with permission from Ref. [76]. 2024 Elsevier.

Patil et al. [77] investigated how different shapes of induction coils affect the temperature profiles during the induction heating of metals. The study examined four coil shapes—classical, conical, square, and oval—using numerical simulations to understand their impact on magnetic flux density and temperature distribution. Each coil shape produced distinct heating patterns, demonstrating that coil geometry significantly influences the efficiency and uniformity of heating. This efficiency is critical in reducing energy consumption and enhancing the performance of induction heating systems.

A study by Martin [78] delves into the application of various additive manufacturing (AM) processes for producing copper induction coils. The author evaluates the use of PBF among several other AM processes and highlights the ability of PBF-LB to produce fully dense and geometrically complex parts necessary for effective induction coils.

5.3. Injection Molding Tools

Copper alloys are ideal for injection molding tooling because they offer a good balance of mechanical strength, hardness, wear resistance, and thermal conductivity. Additive manufacturing enables the integration of geometrically optimized internal cooling channels, which significantly reduces cycle times and enhances production volumes (Figure 15). In injection molds with conformal cooling channels, copper's excellent thermal conductivity allows for faster and more uniform cooling of the mold, reducing cooling times and improving part quality by minimizing warping and residual stresses [79–81].

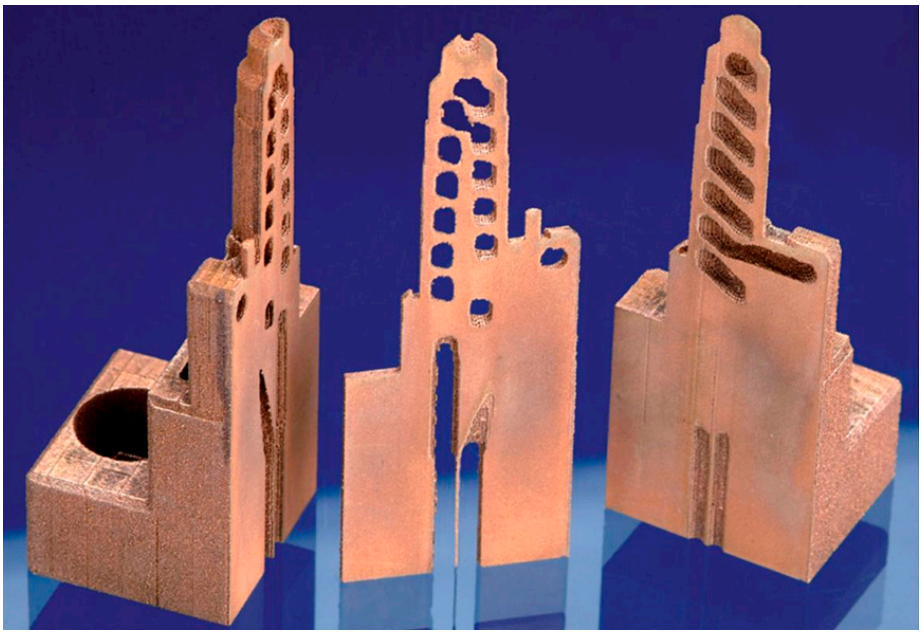

Figure 15. Copper PBF-LB insert with spiral conformal cooling channels for an injection mold, reprinted with permission from ref. [82]. 2024 Elsevier.

The work by Kanbur et al. provides a comprehensive exploration of the use of metal additive manufacturing (AM) techniques for enhancing the cooling processes in plastic injection molds through the integration of conformal cooling channels [81]. The authors study in detail the designs of different CCC types (circular, serpentine, and tapered) integrated into mold inserts. These designs are tailored to closely follow the contours of the mold, significantly enhancing cooling efficiency by providing uniform temperature distribution and reducing cooling times. The precision of PBF-LB allows for the creation of intricate channel geometries that traditional manufacturing could not achieve, which is particularly beneficial for complex mold geometries. The research provides a thorough analysis comparing traditional straight cooling channels with CCCs. The CCCs demonstrate up to 62.9% better cooling performance, underlining their potential to reduce cycle times and improve product quality by minimizing defects like warpage and shrinkage.

Hatos et al. examine the integration of heat-conductive inserts within molds that are fabricated using PBF-LB technology [83]. The study discusses the advantages of conformal cooling channels in injection molding tools, which are designed to follow the mold's geometry more closely than traditional cooling systems. In areas where conformal cooling channels are not feasible or effective, particularly in tightly packed regions of the mold, the integration of heat-conductive inserts made from materials like copper or silver is used. These inserts enhance heat extraction due to their high thermal conductivity. The research highlights a hybrid approach that combines traditional manufacturing techniques with additive manufacturing to optimize mold design. This approach allows for the creation of more complex and efficient cooling geometries that are not possible with conventional methods alone.

5.4. Heat Exchangers and Heat Sinks

Heat exchangers transfer heat between two or more fluids (liquids or gases) while keeping them separate and preventing any mixing. They are often used to heat or cool fluids in various industrial processes. Heat sinks dissipate heat from a solid object (usually an electronic component [84]) to the surrounding environment, preventing overheating [85]. AM enables the production of thermal management devices with optimized cooling channels, which are designed to maximize heat transfer through the exploitation of complex geometries like lattice structures [82,86–88]. Copper's high thermal conductivity makes it ideal for heat dissipation applications in microelectronics, power plants, and transportation [89,90].

Hansjosten et al. present the design and application of innovative AM metallic fluid guiding elements in heat exchangers [91]. The study introduces guiding elements designed using B-spline surfaces that allow for the creation of specific flow patterns within a heat exchanger. These designs aim to maximize heat transfer efficiency while minimizing pressure drop by strategically guiding fluid flows to maintain high local heat transfer throughout the system. The guiding structures are produced by PBF-LB with very thin walls (only 150 µm thick) to minimally obstruct fluid flow while optimizing thermal performance. The functionality of the design is validated through both computational fluid dynamics (CFDs) simulations and experimental data. Results demonstrate that the AM fluid guiding elements significantly enhance heat transfer capabilities compared to traditional designs, with the possibility of reducing the length of pipe-in-pipe heat exchangers drastically.

The work by Kudiiarov et al. focuses on the optimization of the design of heat exchangers and metal hydride bed configurations to enhance the efficiency of hydrogen storage systems [92]. The paper reviews advancements in the heat exchanger design for metal hydride reactors, particularly emphasizing the optimization of heat transfer to improve reactor efficiency. Various configurations of heat exchangers are discussed, including the use of fins and tubes that improve the thermal management within the reactor. Different layouts of metal hydride beds are analyzed to identify how their designs impact the sorption and desorption rates of hydrogen. The study highlights the importance of configuring the metal hydride placement and the heat exchanger design to maximize efficiency and safety in hydrogen storage. PBF-LB can be leveraged to produce heat exchangers with complex geometries that are otherwise difficult to manufacture. AM not only optimizes the heat transfer but also reduces the weight and enhances the performance of metal hydride reactors.

Concerning heat sinks, Constantin et al. explore the capabilities of PBF-LB for producing dense copper parts with a smooth surface using a laser power of 400 W [93]. The printed copper parts achieved near-bulk material properties with a density of 95%, electrical conductivity of 5.71×10^7 S/m, and thermal conductivity of 368 W/mK. These properties make them suitable for high-performance thermal management applications. The study compared the cooling performance of AM heat sinks to a commercial heat sink, showing that the printed structures could cool an electronic chip 45% more efficiently due to their

larger surface area and optimized geometries with columnar elements (Figure 16a), helical tubes (Figure 16b), and bent tubes (Figure 16c).

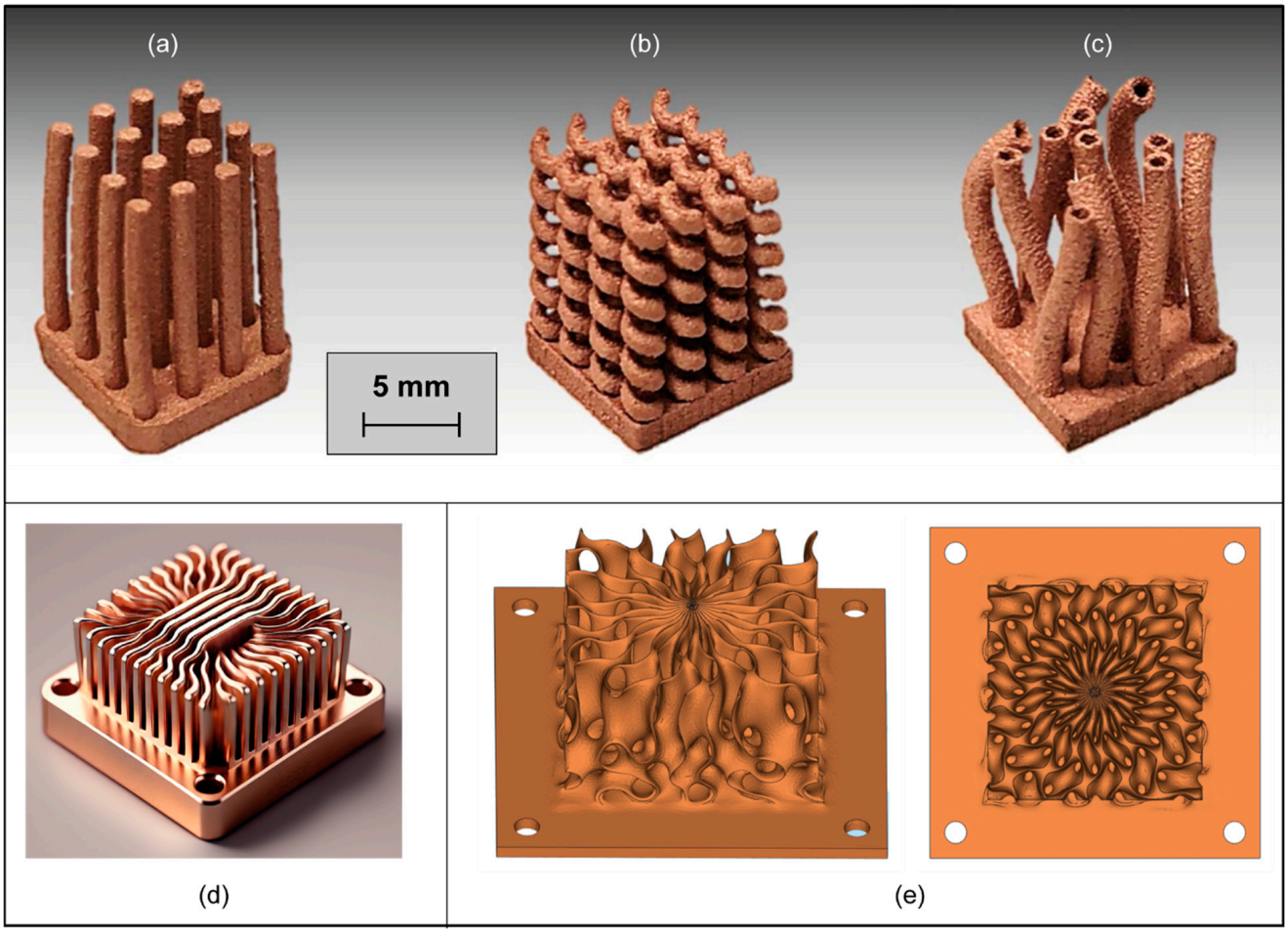

Figure 16. PBF-LB copper heat sink structures with columnar (**a**), helix (**b**), and bent tubes (**c**), adapted with permission from ref. [93]. 2024 Elsevier; heat sinks designed through topology optimization for thermal management of electronic chips (**d**,**e**).

In addition, topology optimization can be used as a design tool to improve the functionality of heat sinks. Topology optimization helps in determining the optimal material distribution within a heat sink, allowing for improved thermal conductivity and heat dissipation. By optimizing the shape and structure, topology optimization can increase the surface area available for heat exchange, which enhances cooling efficiency (Figure 16d). By removing unnecessary material while maintaining structural integrity, topology optimization can produce lighter heat sink designs without compromising performance (Figure 16e).

In their study, Zhang et al. discuss the use of density-based topology optimization to design two-dimensional heat sinks cooled by turbulent natural convection [94]. The methodology involves modifying the governing equations of fluid flow to facilitate topology optimization, integrating material density as a design variable to differentiate between solid and fluid domains within the heat sink. The numerical examples provided show how different parameters, such as the Grashof number and solid thermal conductivity, impact the optimal configurations of heat sinks. The optimization leads to designs that accommodate higher convective flows and improve heat transfer performance by manipulating the geometry based on fluid dynamics and heat transfer simulations.

The work by Alexandersen et al. focused on utilizing topology optimization to design efficient passive cooling systems for LED lamps [95]. The optimized designs were tested against traditional lattice-fin designs and a simple parameter-optimized commercial pin fin design. The results showed that topology-optimized designs had significantly better performance, lowering the LED package temperature by up to 26% compared to traditional designs while using about 12% less material. The authors examined the effects of the orientation (horizontal vs. vertical) of the LED lamps on the cooling performance. It was found that orientation impacts the effectiveness of cooling, with different designs showing varying sensitivities to their positioning.

5.5. Radio Frequency Components

Copper is utilized in the production of vacuum electronic devices, including particle accelerators and microwave electron devices. Additive manufacturing enables the creation of shapes compatible with ultrahigh vacuum conditions, eliminating the need for brazed or diffusion bonds. Vacuum electronic devices (VEDs) provide superior performance compared to solid-state solutions for generating and amplifying radio frequency (RF) signals thanks to their high-power generation and efficiency.

In the literature, several studies have proposed a two-stage process to produce copper RF waveguides and antennas [96–99]. The manufacturing route involves 3D printing of the waveguide structure from a polymer, followed by metal plating to enhance its conductive properties (Figure 17a,b). This type of production may offer flexibility in terms of rapid prototyping and customization for specific application requirements, which are critical for iterative design processes in telecommunications.

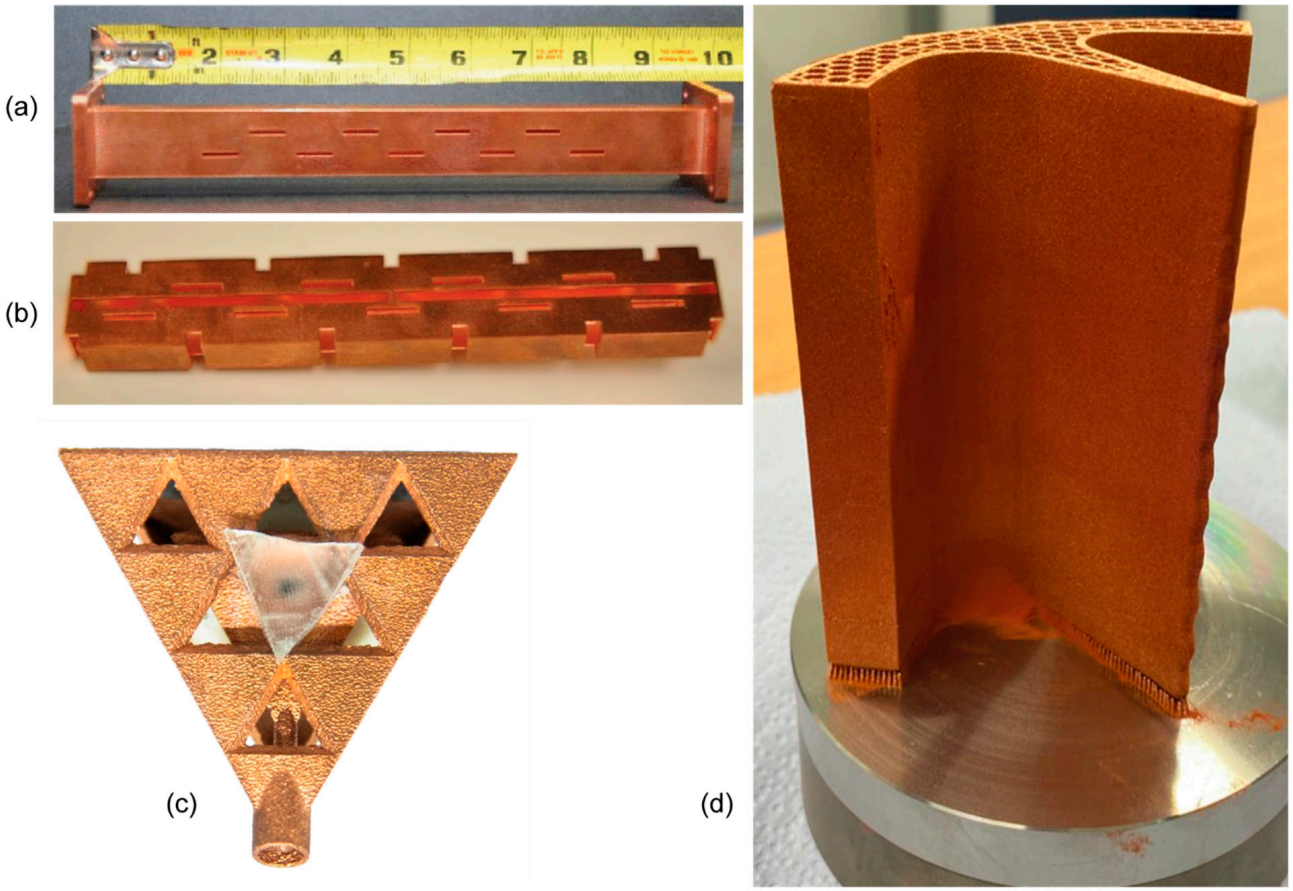

Figure 17. Closed (**a**) and open structure (**b**) of an X-band slot array waveguide, reprinted from Ref. [97]; RF pyramidal antenna with fractal structure manufactured by green laser PBF (**c**), reprinted from Ref. [100]; AM radio frequency quadrupole accelerator (**d**), reprinted from Ref. [101].

As an alternative, Helena et al. proposed the use of a copper filament for extrusion 3D printing of conductive antennas for 5G applications [102]. The conductive filament antenna provided good gain and broader bandwidth compared to those using conductive paint or plating.

Nevertheless, for better performance in the case of high-power applications, solid metal parts are preferred [103]. In their work, Peverini et al. investigated the feasibility of using PBF-LB to create microwave waveguide devices, specifically targeting satellite telecommunications [104]. Their study focuses on producing all-metal components with complex geometries that traditional manufacturing struggles to create efficiently. The research highlighted the need for specific design approaches to optimize PBF use, including adjustments in the orientation of parts to reduce the need for support structures during building and tailoring design to accommodate AM capabilities.

Johnson et al. examined the use of green laser technology in powder bed fusion (PBF) to fabricate a complex fractal antenna [105]. The antenna features a fractal Sierpinski gasket design (Figure 17c) that integrates both conductive and dielectric properties to create a "ship-in-the-bottle" design. This design could only be realized using the capabilities of AM. Concerning the electromagnetic performance, the pyramidal antenna operates effectively within the targeted frequency range, with minimal discrepancies noted in resonant frequencies and impedance measurements.

As regards particle accelerators, Ford et al. presented a comprehensive overview of the integration of metal AM technologies into the production of different parts, such as RF components, beam intercepting devices, and vacuum systems [100]. Torims et al. designed a proof-of-concept prototype for a 750 MHz 4-vane RF quadrupole optimized for PBF-LB [106]. This prototype was manufactured in pure copper, notable for being the first of its kind in the world (Figure 17d). PBF-LB significantly simplified the manufacturing process by eliminating the need for furnace brazing and reducing material waste.

In their studies [101,107], Mayerhofer et al. explored the potential of PBF-LB to produce copper RF cavities with complex internal geometries in a single piece, which traditional manufacturing methods cannot achieve. This approach reduces the need for multiple assembly stages and associated costs. The authors developed co-printed support structures to cope with the difficulties in metal support removal [101]. These supports are designed to be easily removable post-printing through an electrochemical method, enhancing the manufacturability and geometric accuracy of the cavities. The proposed post-processing method also improves the surface roughness of the cavities, which is crucial for achieving high-quality factors in RF applications. These authors also compared the use of red and green laser sources for PBF of the RF cavities for particle accelerators [107]. While both sources achieved the necessary geometric accuracy, red laser PBF demonstrated a slightly higher quality factor efficiency and required less material removal to reach optimal surface conditions.

5.6. Combustion Chambers

Copper and copper alloys are utilized in aerospace applications, including rocket engines and components for space exploration, due to their excellent thermal conductivity and high strength at elevated temperatures. AM allows the creation of intricate designs, improving heat flow and thrust capabilities. Dispersion-strengthened copper alloys GRCop-42 and GRCop-84 are used in rocket combustion chambers for their strength, creep resistance, and fatigue performance at high pressures and temperatures [108].

Metal AM is extensively used in manufacturing critical aerospace components such as liquid-fuel rocket engines, satellite components, and structural elements [9]. These applications benefit from the complex geometries and lightweight designs enabled by AM, leading to improved performance and reduced costs [109]. Significant advantages include the ability to consolidate multiple parts into fewer complex assemblies, reducing weight, and enhancing the functionality of components. This consolidation leads to reduced assembly times and potential failure points [110].

In the past decade, NASA has begun exploring the use of additive manufacturing to create copper combustion chambers for liquid rocket engine applications, with Paul Gradl as one of the most active researchers in this area. In one of their first articles, Gradl et al. focus on the use of PBF-LB to produce combustion chambers out of a copper alloy, specifically the GRCop-84 alloy [108]. They documented extensive hot-fire testing of the AM combustion chambers. These tests evaluated the chambers under operational conditions to assess their performance and durability. In another work, Gradl et al. present the development of thrust chambers using various AM techniques, particularly focusing on the integration of copper alloys and other composite materials [109]. For instance, GRCop-42 alloy was used via PBF-LB to create complex internal structures. While composite overwraps were employed for structural reinforcement and weight reduction, the PBF-LB AM copper alloy chamber was crucial for heat and pressure resistance.

Topology optimization and lattice structure can be used in the design of combustion chambers to improve thermal performance [111]. For example, the repeating cell of triply periodic minimal surface (TPMS) for the gyroid shape enables the creation of inner cooling channels that do not require supports for the PBF-LB process (Figure 18).

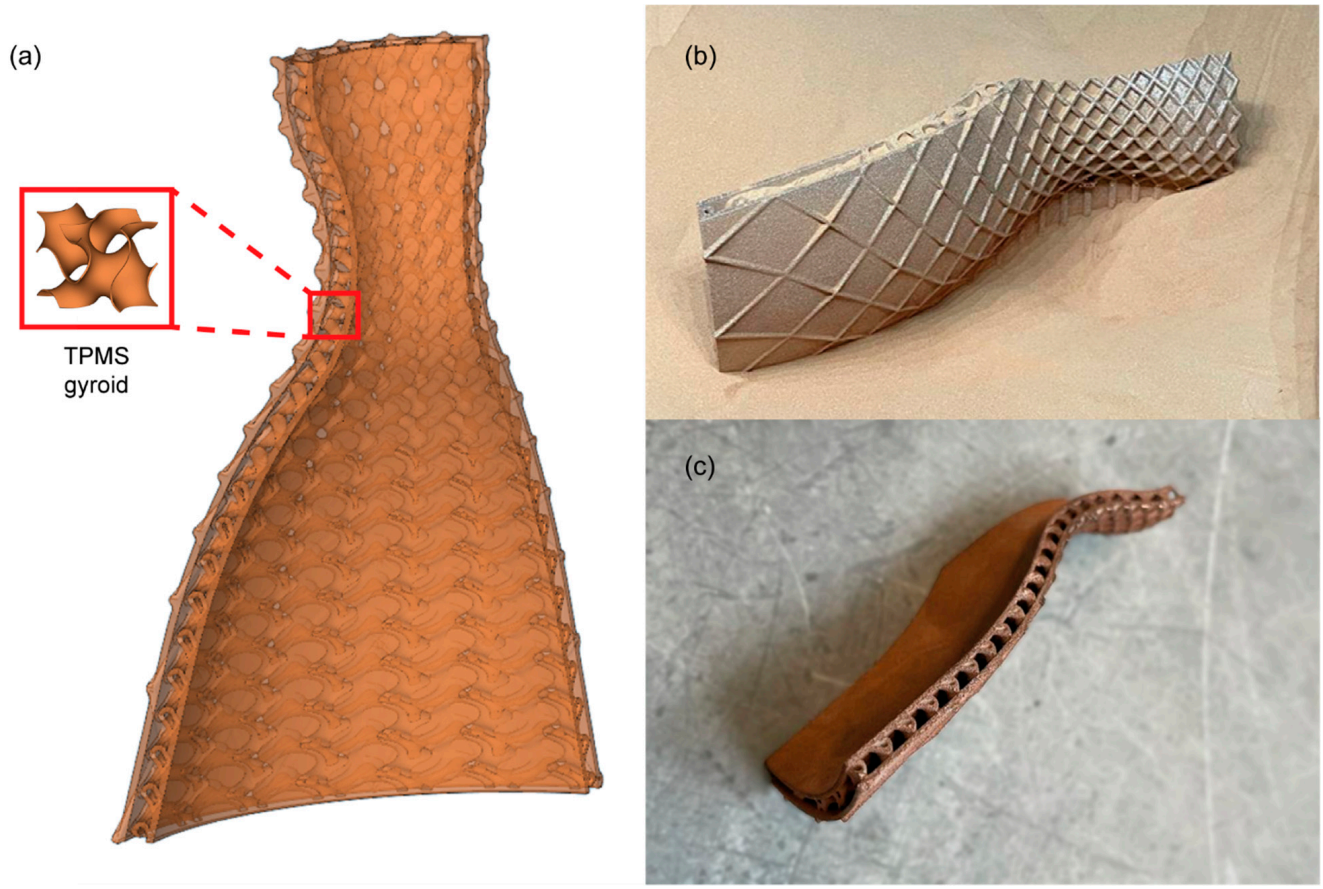

Figure 18. Proof of concept for a combustion chamber with self-supporting TPMS structure for cooling: CAD model (**a**); as-built copper PBF-LB part after powder removal (**b**); finished part after sand blasting (**c**).

Aside from aerospace applications, recently, Sheykhpoor et al. explored the application of AM to enhance the efficiency and integration of components within micro gas turbine systems, particularly for residential and commercial energy applications. The study proposes the integration of the combustor and recuperator to potentially improve system efficiency by up to 5% while significantly reducing the size and weight of the system [112].

Table 3 provides a comparative summary of the different laser sources, as well as the associated processing materials and parameters that are available in the literature for some of the case studies presented above in this section of the paper.

Table 3. Summary of various laser sources, their parameters, and corresponding processing materials used in applications discussed in Section 5.

Copper Part	Figure 12b	Figure 13a	Figure 16a–c	Figure 17c	Figure 17d	Figure 18b
Machine	Aconity Midi (Aconity3D GmbH, Herzogenrath, Germany) + with n Light CFL-1000-SM (nLIGHT, Camas, WA, USA)	Renishaw plc (UK) AM125 (Renishaw plc, Wotton-under-Edge, UK) with a 200-watt D Series laser from SPI Laser (TRUMPF Laser UK Ltd., Southampton, UK)	SLM® 125 3D printer (SLM Solutions Group AG, Lubecca, Germany)	TruPrint 1000 Green Edition with green TruDisk1020 laser (Trumpf SE + Co. KG, Ditzingen, Germany)	TruPrint 1000 Green Edition with green TruDisk1020 laser (Trumpf SE + Co. KG, Ditzingen, Germany)	Prima Additive PrintSharp 250 (Prima Additive S.r.l., Torino, Italy)
Laser wavelength	1070 nm	1070 nm	1070 nm	515 nm	515 nm	1070 nm
Laser power	1000 W	Not declared	400 W	485 W	Preset values from TRUMPF	360 W
Laser spot diameter	Not declared	Not declared	70 µm	200 µm	Preset values from TRUMPF	100 µm
Layer thickness	40 µm	Not declared	30 µm	30 µm	30 µm	30 µm
Laser scan speed	600 mm/s	Not declared	Not declared	600 mm/s	Preset values from TRUMPF	320 mm/s
Hatch spacing	120 µm	Not declared	Not declared	120 µm	Preset values from TRUMPF	100 µm
Material	Pure Copper	Pure Copper	Pure Copper	Copper OFHC (Oxygen-Free High thermal Conductivity)	Copper ETP	CuNi2SiCr
Reference	[68]	[48]	[93]	[100]	[101]	Produced at the IAM Centre of Politecnico di Torino

6. Conclusions

This review summarizes the current state of research on the application of green and blue lasers in PBF-LB technology, with a focus on processing copper and its alloys. These innovative laser sources, characterized by their shorter wavelengths, offer significantly enhanced energy absorption compared to traditional IR lasers. This results in suitable melt pool stability and final density, which are essential for achieving high thermal and electrical conductivity in manufactured components, as specifically shown in Section 4. While some of the results presented here can also be achieved using IR lasers, this is far more challenging due to copper's lower absorption efficiency at longer wavelengths. Achieving similar outcomes with IR lasers often requires significantly higher energy densities, which increases the risk of keyhole pores and other defects due to excessive localized heating.

The use of short-wavelength laser sources may unlock new opportunities in industries like aerospace, automotive, and electronics. Specifically, Section 5 outlines different modern applications of copper and its alloys in PBF-LB, considering both long- and short-wavelength laser sources to cover all explored application solutions. It is possible to expect that future developments will drive a shift in production from IR to green and blue lasers.

Despite their promise, green and blue lasers face challenges, including high costs, limited availability, and the lack of widespread adoption in industrial settings. Future efforts should prioritize optimizing process parameters, improving machine efficiency, and conducting detailed economic and energy impact analyses to promote sustainable adoption. Currently, few commercial PBF-LB machines are equipped with green laser sources. Advancing machine technology and exploring hybrid systems that utilize multiple wavelengths could help combine the benefits of various laser types for even greater performance and efficiency.

By addressing these challenges, green and blue laser technologies can pave the way for more efficient and reliable manufacturing of complex copper and copper alloy components, broadening their applications in high-performance and precision-critical industries.

Author Contributions: Conceptualization, P.M. and L.I.; methodology, P.M.; validation, M.S.K. and A.G.; formal analysis, M.S.K. and A.G.; resources, L.I.; data curation, P.M.; writing—original draft preparation, M.S.K. and A.G.; writing—review and editing, P.M.; visualization, M.S.K. and A.G.; supervision, P.M.; project administration, L.I.; funding acquisition, L.I. All authors have read and agreed to the published version of the manuscript.

Funding: This research was funded by the project "IMplementazione della Produzione Additiva CompetiTiva, IMPACT" co-financed by POR-FESR Piemonte 2014–2020, Azione I.1b.2.2 Bando PiTeF, Piedmont Region.

Acknowledgments: The authors gratefully acknowledge their colleague Flaviana Calignano for the production of the proof of concept of the combustion chamber shown in Figure 18.

Conflicts of Interest: The authors declare no conflicts of interest.

Appendix A

Table A1. Processing windows and main findings explored by previous research using customized PBF-LB machines with green laser. N.D. stands for "not declared".

Material	AM System	Source Laser	Process Parameter	Value	Relative Density	Main Findings	Ref.
Pure copper	Customized PBF-LB/M machine Aconity Mini	Green laser (wavelength 515 nm)	Laser spot diameter [μm]	220	90–100%	126 combinations of different parameters were obtained, of which 12 resulted in densities above 99.95%	[113]
			Hatching distance [μm]	100-200-300			
			Laser power [W]	400-500-600-700-800-900-1000			
			Scanning speed [mm/s]	300-500-800-1000-1500-2000			

Table A1. *Cont.*

Material	AM System	Source Laser	Process Parameter	Value	Relative Density	Main Findings	Ref.
Pure copper	N.D.	Green laser (wavelength 515 nm)	Laser spot diameter [μm]	160	N.D.	Two different copper lattice architectures (octet and cuboctahedron) with dense microstructures and well-defined complex geometries were obtained	[64]
			Hatching distance [μm]	100			
			Laser power [W]	600			
			Scanning speed [mm/s]	1000			
Copper alloy (CuCr1Zr)	Customized AMCM EOS M290	Green qcw-laser (wavelength 532 nm)	Pulse duration [ns]	1.2	85–99.6%	The maximum relative density was measured with a power laser of 125 W, a scanning speed of 400 mm/s, and a hatching speed of 100 μm	[26]
			Laser power [W]	50-75-100-125-150-175-200-300-350-400			
			Scanning speed [mm/s]	400-600-800			
			Hatching distance [μm]	50-70-100			
			Layer thickness [μm]	20			
			Laser spot diameter [μm]	50			
			Laser power [W]	20			
Pure copper	Open PBF-LB system developed in-house, namely Powderful	ns-pulsed single-mode pulsed fiber laser (wavelength 532 nm)	Pulse duration [ns]	1.4	50–98.1%	Larger beam diameters improved density, likely due to the reduction of powder ejection phenomena at lower irradiance levels	[15]
			Laser power [W]	60-80-100			
			Scanning speed [mm/s]	300-600-900			
			Hatching distance [μm]	40-70-100			
			Laser spot diameter [μm]	40-70-100			
			Layer thickness [μm]	50-70			

Table A1. *Cont.*

Material	AM System	Source Laser	Process Parameter	Value	Relative Density	Main Findings	Ref.
Pure copper	Open PBF-LB system developed in-house, namely Powderful	Pulsed active fiber laser with second harmonic generation (wavelength 532 nm)	Pulse duration [ns]	1.4	40–100%	Processability of pure Cu powders with density levels above 99.5%	[105]
			Laser power [W]	40-50			
			Scanning speed [mm/s]	400-500-600			
			Hatching distance [μm]	30-50-70			
			Layer thickness [μm]	50			
Pure copper	Self-constructed, fully automated SLM-module	Green laser (wavelength 515 nm)	Pulse duration [ns]	0.0005	64%	Thin-wall structures with a thickness below 100 μm were achieved. However, the low relative density is mainly due to the limited average power of the setup. The formation of voids is uniformly distributed, regardless of the direction of construction and orientation of the layer during processing	[37]
			Laser power [W]	20			

Table A2. Processing windows and main findings explored by previous research using Trumpf TruPrint 1000 Green Edition (Trumpf SE + Co. KG, Ditzingen, Germany) as AM system (515 nm wavelength green laser). N.D. stands for "not declared".

Material	Process Parameter	Value	Relative Density	Main Findings	References
Pure copper	Hatching distance [μm]	120	96–97%	Nearly dense parts were produced using pure copper powder. However, porosities and over-fusion regions remain in the actual lattice structures, which could be used as highly efficient heat exchangers for hydrogen applications	[55]
	Laser power [W]	485			
	Scanning speed [mm/s]	400-500-600-800-1000-1200			
	Laser spot diameter [μm]	67			
	Layer thickness [μm]	30			

Table A2. *Cont.*

Material	Process Parameter	Value	Relative Density	Main Findings	References
Pure copper	Hatching distance [µm]	100-120-125-150-300	91.6–99.88%	Maximum densification rates are achieved at scan speeds of 400–500 mm/s and laser power higher than 600 W, resulting in improvements of up to 0.3% compared to those obtained with IR lasers. Additionally, a scan speed threshold of approximately 500 mm/s is recommended to prevent process instabilities and porosity	[46]
	Laser power [W]	300-400-500-600-700-800-900-1000			
	Scanning speed [mm/s]	300-400-500-600-700-800			
	Laser spot diameter [µm]	90			
	Layer thickness [µm]	60-100-150			
Copper alloy (Cu4Cr2Nb)	Laser spot diameter [µm]	200	99.98%	A density of 99.98% was achieved by setting a scan speed lower than 900 mm/s, a hatching distance lower than 150 µm, and the layer thickness to 30 µm	[56]
	Hatching distance [µm]	100-150-200-250-300-500			
	Laser power [W]	500			
	Scanning speed [mm/s]	400-500-600-700-800-900-1000-1100-1200			
	Layer thickness [µm]	30-60			
Copper alloy (CuCrZr)	Hatching distance [µm]	90	N.D.	The effect over mechanical and thermal properties of different build orientations were investigated	[61]
	Laser power [W]	485			
	Scanning speed [mm/s]	400			
	Layer thickness [µm]	30			
Copper alloy (CuCrZr)	Hatching distance [µm]	60-70-80-90	96.5–98.69%	The highest mechanical results were encountered with a scan speed of 400 mm/s, a laser power of 485 W, and a hatching distance of 90 µm	[54]
	Laser power [W]	465-475-485-495			
	Scanning speed [mm/s]	300-350-400-450			
	Layer thickness [µm]	30			
Pure copper	Hatching distance [µm]	100-200-500	N.D.	Analysis of multiple PBF-LB tracks indicates that absorptance can be almost doubled, increasing the hatching distance from 100 to 500 µm	[16]
	Laser power [W]	468			
	Scanning speed [mm/s]	500			
	Laser spot diameter [µm]	150			
Pure oxygen-free high thermal conductivity copper (OFHC)	Laser power [W]	100-500 (systematically varied)	N.D.	63 parameter variations were investigated, but regardless of the scanning speed, continuous scan tracks could not be achieved with a laser power of 100 W	[18]
	Scanning speed [mm/s]	50-1100 (systematically varied)			
	Laser spot diameter [µm]	200			

Table A2. *Cont.*

Material	Process Parameter	Value	Relative Density	Main Findings	References
Pure oxygen-free high thermal conductivity copper (OFHC)	Laser power [W]	485	N.D.	The successful fabrication of a geometrically complex and functional antenna was demonstrated. Its surface roughness and conductivity were shown to be almost independent of the build orientation	[100]
	Scanning speed [mm/s]	600			
	Hatching distance [µm]	120			
	Layer thickness [µm]	30			
	Laser spot diameter [µm]	200			
Oxygen-free pure copper (Cu-OF) and oxygenated electrolytic tough pitch copper (Cu-ETP)	Hatching distance [µm]	120	99.98%	Cu-ETP showed slightly higher density values, likely due to its smaller particle size, leading to better packing and increased absorption	[20]
	Layer thickness [µm]	30			
	Line energy input [J/mm]	0.808			
Highly conductive pure copper ETP and copper alloy (CuCr1Zr)	Volume Energy [J/mm^3]	225	99.8%	A stable PBF-LB process was achieved that improves process efficiency and build rate for both pure copper and low alloy copper	[21]
	Layer thickness [µm]	30			

References

1. Calignano, F.; Manfredi, D.; Ambrosio, E.P.; Biamino, S.; Lombardi, M.; Atzeni, E.; Salmi, A.; Minetola, P.; Iuliano, L.; Fino, P. Overview on Additive Manufacturing Technologies. *Proc. IEEE* **2017**, *105*, 593–612. [CrossRef]
2. Kruth, J.-P.; Leu, M.C.; Nakagawa, T. Progress in Additive Manufacturing and Rapid Prototyping. *CIRP Ann.* **1998**, *47*, 525–540. [CrossRef]
3. Muralidhara, H.B.; Banerjee, S. *3D Printing Technology and Its Diverse Applications*; Apple Academic Press: Boca Raton, FL, USA, 2021; ISBN 9781003145349.
4. Armstrong, M.; Mehrabi, H.; Naveed, N. An Overview of Modern Metal Additive Manufacturing Technology. *J. Manuf. Process* **2022**, *84*, 1001–1029. [CrossRef]
5. Zhang, Y.; Jarosinski, W.; Jung, Y.-G.; Zhang, J. 2—Additive Manufacturing Processes and Equipment. In *Additive Manufacturing*; Zhang, J., Jung, Y.-G., Eds.; Butterworth-Heinemann: Oxford, UK, 2018; pp. 39–51, ISBN 978-0-12-812155-9.
6. *ASTM F3177-21*; Additive Manufacturing—General Principles—Fundamentals and Vocabulary. ASTM International: West Conshohocken, PA, USA, 2021.
7. *ISO 52900:2021*; Additive Manufacturing—General Principles—Fundamentals and Vocabulary. ISO: Geneva, Switzerland, 2021.
8. Schneck, M.; Gollnau, M.; Lutter-Günther, M.; Haller, B.; Schlick, G.; Lakomiec, M.; Reinhart, G. Evaluating the Use of Additive Manufacturing in Industry Applications. *Procedia CIRP* **2019**, *81*, 19–23. [CrossRef]
9. Blakey-Milner, B.; Gradl, P.; Snedden, G.; Brooks, M.; Pitot, J.; Lopez, E.; Leary, M.; Berto, F.; du Plessis, A. Metal Additive Manufacturing in Aerospace: A Review. *Mater. Des.* **2021**, *209*, 110008. [CrossRef]
10. SciVal. Available online: https://www.elsevier.com/products/scival (accessed on 24 July 2024).
11. De Terris, T.; Baffie, T.; Ribière, C. Additive Manufacturing of Pure Copper: A Review and Comparison of Physical, Microstructural, and Mechanical Properties of Samples Manufactured with Laser-Powder Bed Fusion (L-PBF), Electron Beam Melting (EBM) and Metal Fused Deposition Modelling (MFDM) Technologies. *Int. J. Mater. Form.* **2023**, *16*, 32. [CrossRef]
12. Ribeiro, K.S.B.; Mariani, F.E.; Coelho, R.T. A Study of Different Deposition Strategies in Direct Energy Deposition (DED) Processes. *Procedia Manuf.* **2020**, *48*, 663–670. [CrossRef]
13. Stepien, L.; Gruber, S.; Greifzu, M.; Riede, M.; Roch, A. Pure Copper: Advanced Additive Manufacturing. In *Advanced Additive Manufacturing*; Shishkovsky, I.V., Ed.; IntechOpen: Rijeka, Croatia, 2022; Chapter 11; ISBN 978-1-83962-821-4.
14. Bar-Kohany, T.; Jain, A. Dissipation of Boundary Effects in Multilayer Heat Conduction Problems. *Int. J. Heat Mass Transf.* **2024**, *223*, 125207. [CrossRef]
15. Singh, A.; Caprio, L.; Previtali, B.; Demir, A.G. Processability of Pure Cu by LPBF Using a Ns-Pulsed Green Fiber Laser. *Opt. Laser Technol.* **2022**, *154*, 108310. [CrossRef]

16. Nordet, G.; Gorny, C.; Mayi, Y.; Daligault, J.; Dal, M.; Effernelli, A.; Blanchet, E.; Coste, F.; Peyre, P. Absorptivity Measurements during Laser Powder Bed Fusion of Pure Copper with a 1 KW Cw Green Laser. *Opt. Laser Technol.* **2022**, *147*, 107612. [CrossRef]
17. Stoll, T.; Kirstein, M.; Franke, J. Additive Manufacturing of 3D-Copper-Metallizations on Alumina by Means of Selective Laser Melting for Power Electronic Applications. In Proceedings of the CIPS 2018, 10th International Conference on Integrated Power Electronics Systems, Stuttgart, Germany, 20–22 March 2018; pp. 1–6.
18. Horn, M.; Schmitt, M.; Schafnitzel, M.; van Husen, A.; Wagenblast, P.; Auernhammer, S.; Heyder, J.; Hauck, C.; Barz, J.; Ott, M.; et al. Powder Bed Fusion of Highly Filigree Copper Features Using a Green Laser. *Procedia CIRP* **2022**, *111*, 81–86. [CrossRef]
19. Gallagher, C.; Kerr, E.; McFadden, S. Particle Size Distribution for Additive Manufacturing Powder Using Stereological Corrections. *Powder Technol.* **2023**, *429*, 118873. [CrossRef]
20. Gruber, S.; Stepien, L.; López, E.; Brueckner, F.; Leyens, C. Physical and Geometrical Properties of Additively Manufactured Pure Copper Samples Using a Green Laser Source. *Materials* **2021**, *14*, 3642. [CrossRef]
21. Wagenblast, P.; Myrell, A.; Thielmann, M.; Scherbaum, T.; Coupek, D. Additive Manufacturing with Green Disk Lasers. *Proc. SPIE* **2020**, *11271*, 112710J.
22. Jadhav, S.D.; Fu, D.; Deprez, M.; Ramharter, K.; Willems, D.; Van Hooreweder, B.; Vanmeensel, K. Highly Conductive and Strong CuSn0.3 Alloy Processed via Laser Powder Bed Fusion Starting from a Tin-Coated Copper Powder. *Addit. Manuf.* **2020**, *36*, 101607. [CrossRef]
23. Zheng, R.; Cui, J.; Yang, Y.; Li, S.; Misra, R.D.K.; Kondoh, K.; Zhu, Q.; Lu, Y.; Li, X. Enhanced Densification of Copper during Laser Powder Bed Fusion through Powder Surface Alloying. *J. Mater. Process Technol.* **2022**, *305*, 117575. [CrossRef]
24. Jadhav, S.D.; Dhekne, P.P.; Brodu, E.; Van Hooreweder, B.; Dadbakhsh, S.; Kruth, J.P.; van Humbeeck, J.; Vanmeensel, K. Laser Powder Bed Fusion Additive Manufacturing of Highly Conductive Parts Made of Optically Absorptive Carburized CuCr1 Powder. *Mater. Des.* **2021**, *198*. [CrossRef]
25. Tiberto, D.; Klotz, U.E.; Held, F.; Wolf, G. Additive Manufacturing of Copper Alloys: Influence of Process Parameters and Alloying Elements. *Mater. Sci. Technol.* **2019**, *35*, 969–977. [CrossRef]
26. von Lintel, H.; Evsiutkina, E.; Haase, C.; Krupp, U.; Jahns, K. Copper Alloys for Additive Manufacturing: Laser Powder Bed Fusion of CuCr1Zr by Using a Green Qcw-Laser. *Eur. J. Mater.* **2023**, *3*, 2115945. [CrossRef]
27. Sefene, E.M. State-of-the-Art of Selective Laser Melting Process: A Comprehensive Review. *J. Manuf. Syst.* **2022**, *63*, 250–274. [CrossRef]
28. Stoll, T.; Trautnitz, P.; Schmiedeke, S.; Franke, J.; Travitzky, N. Process Development for Laser Powder Bed Fusion of Pure Copper. In Proceedings of the Laser 3D Manufacturing VII, San Francisco, CA, USA, 4–6 February 2020.
29. Colopi, M.; Demir, A.G.; Caprio, L.; Previtali, B. Limits and Solutions in Processing Pure Cu via Selective Laser Melting Using a High-Power Single-Mode Fiber Laser. *Int. J. Adv. Manuf. Technol.* **2019**, *104*, 2473–2486. [CrossRef]
30. Mattern, M.; Kukreja, L.M.; Ostendorf, A. Temperature-Dependent Reflectance of Copper with Different Surface Conditions Measured at 1064 Nm. *J. Mater. Eng. Perform.* **2024**, *33*, 2897–2909. [CrossRef]
31. Fiedler, T.; Jähnig Domingues, M.; Winter, C.; Rösler, J. High Conductive Copper Alloys for Additive Manufacturing. *Prog. Addit. Manuf.* **2024**, *9*, 1643–1652. [CrossRef]
32. Wijaya, A.; Wagner, J.; Sartory, B.; Brunner, R. Analyzing Microstructure Relationships in Porous Copper Using a Multi-Method Machine Learning-Based Approach. *Commun. Mater.* **2024**, *5*, 59. [CrossRef]
33. Wei, M.; Ding, W.J.; Vastola, G.; Zhang, Y.-W. Quantitative Study on the Dynamics of Melt Pool and Keyhole and Their Controlling Factors in Metal Laser Melting. *Addit. Manuf.* **2022**, *54*, 102779. [CrossRef]
34. Engler, S.; Ramsayer, R.; Poprawe, R. Process Studies on Laser Welding of Copper with Brilliant Green and Infrared Lasers. *Phys. Procedia* **2011**, *12*, 339–346. [CrossRef]
35. Chung, W.-S.; Olowinsky, A.; Gillner, A. Process Studies on Copper Laser Beam Welding over Gap by Using Disc Laser at Green Wavelength. *J. Adv. Join. Process.* **2020**, *1*, 100009. [CrossRef]
36. Kohl, S.; Kaufmann, F.; Schmidt, M. Why Color Matters—Proposing a Quantitative Stability Criterion for Laser Beam Processing of Metals Based on Their Fundamental Optical Properties. *Metals* **2022**, *12*, 1118. [CrossRef]
37. Kaden, L.; Matthäus, G.; Ramm, R.; Ullsperger, T.; Seyfarth, B.; Nolte, S. Additive Manufacturing of Pure Copper Using Ultrashort Laser Pulses. *Proc. SPIE* **2019**, *10909*, 109090D.
38. Fu, E.; Spiegelhalder, R.; Vogt, S.; Goebel, M. The Best Kept Secret in Laser Additive Manufacturing: Green Lasers, a Unique Innovation. *Proc. SPIE* **2022**, *11992*, 1199202.
39. Hori, E.; Sato, Y.; Shibata, T.; Tojo, K.; Tsukamoto, M. Development of SLM Process Using 200 W Blue Diode Laser for Pure Copper Additive Manufacturing of High Density Structure. *J. Laser Appl.* **2020**, *33*, 012008. [CrossRef]
40. Jedamzik, R.; Carré, A.; Hagemann, V.; Bartelmess, L.; Leukel, S.; Petzold, U. Optical Materials for Blue-Laser Processing. In Proceedings of the Optical Engineering + Applications, San Diego, CA, USA, 1–5 August 2021.
41. Qi, Z.; Chen, C.; Wang, C.; Zhou, Z.; Zhou, J.; Long, Y. Effect of Different Laser Wavelengths on Laser Cladding of Pure Copper. *Surf. Coat. Technol.* **2023**, *454*, 129181. [CrossRef]
42. Lu, P.; Cheng-Lin, Z.; Tong, L.; Xin-Yu, L.; Jiang-Lin, L.; Shun, L.; Wen-Hao, W.; Heng-Hua, Z. Molten Pool Structure and Temperature Flow Behavior of Green-Laser Powder Bed Fusion Pure Copper. *Mater. Res. Express* **2022**, *9*, 016504. [CrossRef]
43. Tang, X.; Chen, X.; Sun, F.; Liu, P.; Zhou, H.; Fu, S. The Current State of CuCrZr and CuCrNb Alloys Manufactured by Additive Manufacturing: A Review. *Mater. Des.* **2022**, *224*, 111419. [CrossRef]

44. Liu, X.; Wang, H.; Kaufmann, K.; Vecchio, K. Directed Energy Deposition of Pure Copper Using Blue Laser. *J. Manuf. Process.* **2023**, *85*, 314–322. [CrossRef]
45. Jadhav, S.D.; Dadbakhsh, S.; Vleugels, J.; Hofkens, J.; Van Puyvelde, P.; Yang, S.; Kruth, J.-P.; Van Humbeeck, J.; Vanmeensel, K. Influence of Carbon Nanoparticle Addition (and Impurities) on Selective Laser Melting of Pure Copper. *Materials* **2019**, *12*, 2469. [CrossRef] [PubMed]
46. Nordet, G.; Gorny, C.; Coste, F.; Lapouge, P.; Effernelli, A.; Blanchet, E.; Peyre, P. Influence of Laser Wavelength on the Powder Bed Fusion of Pure Copper. *Prog. Addit. Manuf.* **2024**, *in press*. [CrossRef]
47. Jadhav, S.D.; Dadbakhsh, S.; Goossens, L.; Kruth, J.-P.; Van Humbeeck, J.; Vanmeensel, K. Influence of Selective Laser Melting Process Parameters on Texture Evolution in Pure Copper. *J. Mater. Process. Technol.* **2019**, *270*, 47–58. [CrossRef]
48. Silbernagel, C.; Gargalis, L.; Ashcroft, I.; Hague, R.; Galea, M.; Dickens, P. Electrical Resistivity of Pure Copper Processed by Medium-Powered Laser Powder Bed Fusion Additive Manufacturing for Use in Electromagnetic Applications. *Addit. Manuf.* **2019**, *29*, 100831. [CrossRef]
49. Abdelhafiz, M.; Al-Rubaie, K.S.; Emadi, A.; Elbestawi, M.A. Process–Structure–Property Relationships of Copper Parts Manufactured by Laser Powder Bed Fusion. *Materials* **2021**, *14*, 2945. [CrossRef] [PubMed]
50. Fang, X.; Xia, W.; Wei, Q.; Wu, Y.; Lv, W.; Guo, W. Preparation of Cu-Cr-Zr Alloy by Laser Powder Bed Fusion: Parameter Optimization, Microstructure, Mechanical and Thermal Properties for Microelectronic Applications. *Metals* **2021**, *11*, 1410. [CrossRef]
51. Qu, S.; Ding, J.; Fu, J.; Fu, M.; Zhang, B.; Song, X. High-Precision Laser Powder Bed Fusion Processing of Pure Copper. *Addit. Manuf.* **2021**, *48*, 102417. [CrossRef]
52. Wallis, C.; Buchmayr, B. Effect of Heat Treatments on Microstructure and Properties of CuCrZr Produced by Laser-Powder Bed Fusion. *Mater. Sci. Eng. A* **2019**, *744*, 215–223. [CrossRef]
53. Huang, Y.; Fleming, T.G.; Clark, S.J.; Marussi, S.; Fezzaa, K.; Thiyagalingam, J.; Leung, C.L.A.; Lee, P.D. Keyhole Fluctuation and Pore Formation Mechanisms during Laser Powder Bed Fusion Additive Manufacturing. *Nat. Commun.* **2022**, *13*, 1170. [CrossRef]
54. Tang, X.; Chen, X.; Sun, F.; Li, L.; Liu, P.; Zhou, H.; Fu, S.; Li, A. A Study on the Mechanical and Electrical Properties of High-Strength CuCrZr Alloy Fabricated Using Laser Powder Bed Fusion. *J. Alloys Compd.* **2022**, *924*, 166627. [CrossRef]
55. Zaied, M.; Msolli, S.; Fourment, H.; Aubry, E.; Bolot, R.; Lebaal, N.; Fenineche, N.; Promoppatum, P. The Contribution of 515-Nm Green Laser L-PBF to the Thermal Performance of Lattice-Based Heat Exchangers for Hydrogen Storage Applications. *Int. J. Adv. Manuf. Technol.* **2024**, *133*, 1501–1518. [CrossRef]
56. Zhang, W.-J.; Huang, L.; Mi, X.-J.; Xie, H.-F.; Feng, X.; Ahn, J.H. Researches for Higher Electrical Conductivity Copper-Based Materials. *cMat* **2024**, *1*, e13. [CrossRef]
57. Gruber, S.; Stepien, L.; Gerdt, L.; Lopez, E.; Kieser, J.; Brueckner, F.; Leyens, C.; Bratt, C. Process Development for Laser Powder Bed Fusion of GRCop-42 Using a 515 Nm Laser Source. *J. Laser Appl.* **2023**, *35*, 042078. [CrossRef]
58. Wegener, T.; Koopmann, J.; Richter, J.; Krooß, P.; Niendorf, T. CuCrZr Processed by Laser Powder Bed Fusion—Processability and Influence of Heat Treatment on Electrical Conductivity, Microstructure and Mechanical Properties. *Fatigue Fract. Eng. Mater. Struct.* **2021**, *44*, 2570–2590. [CrossRef]
59. Franz, R.; Wiedemann, G. Ueber Die Wärme-Leitungsfähigkeit Der Metalle. *Ann. Phys.* **1853**, *165*, 497–531. [CrossRef]
60. Huang, Y.; Su, Y.; Guo, X.; Guo, Q.; Ouyang, Q.; Zhang, G.; Zhang, D. Fabrication and Thermal Conductivity of Copper Coated Graphite Film/Aluminum Composites for Effective Thermal Management. *J. Alloys Compd.* **2017**, *711*, 22–30. [CrossRef]
61. Xie, H.; Tang, X.; Chen, X.; Sun, F.; Dong, L.; Tan, Y.; Chu, H.; Zhou, H.; Liu, P.; Fu, S. The Effect of Build Orientations on Mechanical and Thermal Properties on CuCrZr Alloys Fabricated by Laser Powder Bed Fusion. *J. Mater. Res. Technol.* **2023**, *23*, 3322–3336. [CrossRef]
62. Krakhmalev, P.; Kazantseva, N. 8—Microstructure of L-PBF Alloys. In *Fundamentals of Laser Powder Bed Fusion of Metals*; Yadroitsev, I., Yadroitsava, I., du Plessis, A., MacDonald, E., Eds.; Elsevier: Amsterdam, The Netherlands, 2021; pp. 215–243, ISBN 978-0-12-824090-8.
63. Wang, M.; Li, R.; Yuan, T.; Chen, C.; Zhang, M.; Weng, Q.; Yuan, J. Selective Laser Melting of W-Ni-Cu Composite Powder: Densification, Microstructure Evolution and Nano-Crystalline Formation. *Int. J. Refract. Met. Hard Mater.* **2018**, *70*, 9–18. [CrossRef]
64. Kang, S.-G.; Gainov, R.; Heußen, D.; Bieler, S.; Sun, Z.; Weinberg, K.; Dehm, G.; Ramachandramoorthy, R. Green Laser Powder Bed Fusion Based Fabrication and Rate-Dependent Mechanical Properties of Copper Lattices. *Mater. Des.* **2023**, *231*, 112023. [CrossRef]
65. Jiang, Q.; Zhang, P.; Yu, Z.; Shi, H.; Wu, D.; Yan, H.; Ye, X.; Lu, Q.; Tian, Y. A Review on Additive Manufacturing of Pure Copper. *Coatings* **2021**, *11*, 740. [CrossRef]
66. Szabó, L.; Fodor, D. The Key Role of 3D Printing Technologies in the Further Development of Electrical Machines. *Machines* **2022**, *10*, 330. [CrossRef]
67. Selema, A.; Ibrahim, M.N.; Sergeant, P. Metal Additive Manufacturing for Electrical Machines: Technology Review and Latest Advancements. *Energies* **2022**, *15*, 1076. [CrossRef]
68. Putz, C.; Reich, S.; Ziegler, S.; Schleifenbaum, J.H.; Bajah, Y.; Buscher, M. Hybrid PBF-LB/M of Pure Copper for Hairpin Winding Heads of Electric Traction Drives. *BHM Berg- Und Hüttenmännische Monatshefte* **2024**, *169*, 23–30. [CrossRef]

69. Simpson, N.; Munagala, S.P.; Catania, A.; Derguti, F.; Mellor, P.H. Functionally Graded Electrical Windings Enabled by Additive Manufacturing. In Proceedings of the 2022 International Conference on Electrical Machines (ICEM), Valencia, Spain, 5–8 September 2022; pp. 1477–1483.
70. Ranjan, R.; Tangudu, J. Thermal Design of High Power-Density Additively-Manufactured Induction Motors. In Proceedings of the 2014 IEEE Energy Conversion Congress and Exposition (ECCE), Pittsburgh, PA, USA, 14–18 September 2014; pp. 1325–1331.
71. Sarap, M.; Kallaste, A.; Shams Ghahfarokhi, P.; Tiismus, H.; Vaimann, T. Utilization of Additive Manufacturing in the Thermal Design of Electrical Machines: A Review. *Machines* **2022**, *10*, 251. [CrossRef]
72. Schuhmann, D.; Rockinger, C.; Merkel, M.; Harrison, D.K. A Study on Additive Manufacturing for Electromobility. *World Electr. Veh. J.* **2022**, *13*, 154. [CrossRef]
73. Chen, P.; Shi, Y.; Zhang, L.; Li, J.; Zhu, X.; Fu, Q.; Liao, Q. Performance of a Thermally Regenerative Battery with 3D-Printed Cu/C Composite Electrodes: Effect of Electrode Pore Size. *Ind. Eng. Chem. Res.* **2020**, *59*, 21286–21293. [CrossRef]
74. Martinez, A.C.; Maurel, A.; Yelamanchi, B.; Talin, A.A.; Grugeon, S.; Panier, S.; Dupont, L.; Aranzola, A.; Schiaffino, E.; Sreenivasan, S.T.; et al. Combining 3D Printing of Copper Current Collectors and Electrophoretic Deposition of Electrode Materials for Structural Lithium-Ion Batteries. *Adv. Manuf.* **2024**. [CrossRef]
75. Cagliano, A.C.; Mangano, G.; Rafele, C.; Carlin, A. Lithium-Ion Battery Procurement Strategies: Evidence from the Automotive Field. *IFAC-Pap.* **2020**, *53*, 12688–12694. [CrossRef]
76. Järvenpää, A.; Kim, D.B.; Mäntyjärvi, K. Chapter 14—Metal Additive Manufacturing. In *Welding of Metallic Materials*; Khoshnaw, F., Ed.; Elsevier: Amsterdam, The Netherlands, 2023; pp. 493–536, ISBN 978-0-323-90552-7.
77. Patil, M.; Kumar Choubey, R.; Kumar Jain, P. Influence of Coil Shapes on Temperature Distribution in Induction Heating Process. *Mater. Today Proc.* **2023**, *72*, 3029–3035. [CrossRef]
78. Martin, J.D. Exploring Additive Manufacturing Processes for Direct 3D Printing of Copper Induction Coils. In Proceedings of the ASME 2017 International Mechanical Engineering Congress and Exposition, Tampa, FL, USA, 3–9 November 2017.
79. Arman, S.; Lazoglu, I. A Comprehensive Review of Injection Mold Cooling by Using Conformal Cooling Channels and Thermally Enhanced Molds. *Int. J. Adv. Manuf. Technol.* **2023**, *127*, 2035–2106. [CrossRef]
80. Tan, C.; Wang, D.; Ma, W.; Chen, Y.; Chen, S.; Yang, Y.; Zhou, K. Design and Additive Manufacturing of Novel Conformal Cooling Molds. *Mater. Des.* **2020**, *196*, 109147. [CrossRef]
81. Kanbur, B.B.; Suping, S.; Duan, F. Design and Optimization of Conformal Cooling Channels for Injection Molding: A Review. *Int. J. Adv. Manuf. Technol.* **2020**, *106*, 3253–3271. [CrossRef]
82. McDonough, J.R. A Perspective on the Current and Future Roles of Additive Manufacturing in Process Engineering, with an Emphasis on Heat Transfer. *Therm. Sci. Eng. Prog.* **2020**, *19*, 100594. [CrossRef]
83. Hatos, I.; Kocsis, B.; Hargitai, H. Conformal Cooling with Heat-Conducting Inserts by Direct Metal Laser Sintering. *IOP Conf. Ser. Mater. Sci. Eng.* **2018**, *448*, 12027. [CrossRef]
84. Pilagatti, A.N.; Piscopo, G.; Atzeni, E.; Iuliano, L.; Salmi, A. Design of Additive Manufactured Passive Heat Sinks for Electronics. *J. Manuf. Process.* **2021**, *64*, 878–888. [CrossRef]
85. Sciacca, G.; Sinico, M.; Cogo, G.; Bigolaro, D.; Pepato, A.; Esposito, J. Experimental and Numerical Characterization of Pure Copper Heat Sinks Produced by Laser Powder Bed Fusion. *Mater. Des.* **2022**, *214*, 110415. [CrossRef]
86. Dutkowski, K.; Kruzel, M.; Rokosz, K. Review of the State-of-the-Art Uses of Minimal Surfaces in Heat Transfer. *Energies* **2022**, *15*, 7994. [CrossRef]
87. Mahmoud, D.; Tandel, S.R.S.; Yakout, M.; Elbestawi, M.; Mattiello, F.; Paradiso, S.; Ching, C.; Zaher, M.; Abdelnabi, M. Enhancement of Heat Exchanger Performance Using Additive Manufacturing of Gyroid Lattice Structures. *Int. J. Adv. Manuf. Technol.* **2023**, *126*, 4021–4036. [CrossRef]
88. Anwajler, B. Potential of 3D Printing for Heat Exchanger Heat Transfer Optimization—Sustainability Perspective. *Inventions* **2024**, *9*, 60. [CrossRef]
89. Careri, F.; Khan, R.H.U.; Todd, C.; Attallah, M.M. Additive Manufacturing of Heat Exchangers in Aerospace Applications: A Review. *Appl. Therm. Eng.* **2023**, *235*, 121387. [CrossRef]
90. Choong, Y.H.; Krishnan, M.; Gupta, M. Recent Advances in the 3D Printing of Pure Copper Functional Structures for Thermal Management Devices. *Technologies* **2023**, *11*, 141. [CrossRef]
91. Hansjosten, E.; Wenka, A.; Hensel, A.; Benzinger, W.; Klumpp, M.; Dittmeyer, R. Custom-Designed 3D-Printed Metallic Fluid Guiding Elements for Enhanced Heat Transfer at Low Pressure Drop. *Chem. Eng. Process.-Process Intensif.* **2018**, *130*, 119–126. [CrossRef]
92. Kudiiarov, V.; Elman, R.; Pushilina, N.; Kurdyumov, N. State of the Art in Development of Heat Exchanger Geometry Optimization and Different Storage Bed Designs of a Metal Hydride Reactor. *Materials* **2023**, *16*, 4891. [CrossRef] [PubMed]
93. Constantin, L.; Wu, Z.; Li, N.; Fan, L.; Silvain, J.-F.; Lu, Y.F. Laser 3D Printing of Complex Copper Structures. *Addit. Manuf.* **2020**, *35*, 101268. [CrossRef]
94. Zhang, B.; Zhu, J.; Gong, L.; Jia, K.; Gao, L. Topology Optimization of Heat Sink in Turbulent Natural Convection Using K-ω Turbulent Model. *Appl. Math. Model.* **2023**, *118*, 272–302. [CrossRef]
95. Alexandersen, J.; Sigmund, O.; Meyer, K.E.; Lazarov, B.S. Design of Passive Coolers for Light-Emitting Diode Lamps Using Topology Optimisation. *Int. J. Heat Mass Transf.* **2018**, *122*, 138–149. [CrossRef]

96. Lomakin, K.; Simon, D.; Sippel, M.; Helmreich, K.; Seler, E.; Tong, Z.; Reuter, R.; Gold, G. 3D Printed Slotted Waveguide Array Antenna for Automotive Radar Applications in W-Band. In Proceedings of the 2018 15th European Radar Conference (EuRAD), Madrid, Spain, 26–28 September 2018; pp. 389–392.
97. Sage, G.P. Le 3D Printed Waveguide Slot Array Antennas. *IEEE Access* **2016**, *4*, 1258–1265. [CrossRef]
98. Le Sage, G.P. Thermal Frequency Drift of 3D Printed Microwave Components. *Metals* **2020**, *10*, 580. [CrossRef]
99. Koul, S.K.; Swapna, S.; Karthikeya, G.S. Additive Manufacturing in Antenna Development. In *Antenna Systems for Modern Wireless Devices*; Koul, S.K., Swapna, S., Karthikeya, G.S., Eds.; Springer Nature: Singapore, 2024; pp. 283–319, ISBN 978-981-97-3369-9.
100. Ford, D.; Bonesso, M.; Caforio, R.; Candela, S.; Candela, V.; Chyhyrynets, E.; Dima, R.; Favero, G.; Keppel, G.; Pepato, A.; et al. Additive Manufacturing of Pure Niobium and Copper Using Laser Powder Bed Fusion for Particle Accelerator Applications. *JACoW* **2023**, *SRF2023*, WEPWB119. [CrossRef]
101. Mayerhofer, M.; Brenner, S.; Doppler, M.; Catarino, L.; Girst, S.; Nedeljkovic-Groha, V.; Dollinger, G. Improving Fabrication and Performance of Additively Manufactured RF Cavities by Employing Co-Printed Support Structures and Their Subsequent Removal. *Instruments* **2024**, *8*, 18. [CrossRef]
102. Helena, D.; Ramos, A.; Varum, T.; Matos, J.N. The Use of 3D Printing Technology for Manufacturing Metal Antennas in the 5G/IoT Context. *Sensors* **2021**, *21*, 3321. [CrossRef] [PubMed]
103. Martín-Iglesias, P.; Marechal, M.; Calves, P.; Hazard, M.; Pambaguian, L.; Brandao, A.; Rodriguez Castillo, S.; Martin, T.; Percaz, J.; Iza, V.; et al. Metal 3D Printing for RF/Microwave High-Frequency Parts. *CEAS Space J.* **2023**, *15*, 7–25. [CrossRef]
104. Peverini, O.A.; Lumia, M.; Calignano, F.; Addamo, G.; Lorusso, M.; Ambrosio, E.P.; Manfredi, D.; Virone, G. Selective Laser Melting Manufacturing of Microwave Waveguide Devices. *Proc. IEEE* **2017**, *105*, 620–631. [CrossRef]
105. Johnson, K.; Burden, E.; Shaffer, M.; Noack, T.; Mueller, M.; Walker, J.; MacDonald, E.; Cortes, P.; Quintana, J. A Copper Pyramidal Fractal Antenna Fabricated with Green-Laser Powder Bed Fusion. *Prog. Addit. Manuf.* **2022**, *7*, 931–942. [CrossRef]
106. Torims, T.; Pikurs, G.; Gruber, S.; Vretenar, M.; Ratkus, A.; Vedani, M.; López, E.; Brückner, F. First Proof-of-Concept Prototype of an Additive Manufactured Radio Frequency Quadrupole. *Instruments* **2021**, *5*, 35. [CrossRef]
107. Mayerhofer, M.; Brenner, S.; Dickmann, M.; Doppler, M.; Gruber, S.; Helm, R.; Lopez, E.; Maier, V.; Mitteneder, J.; Neukirchen, C.; et al. Red and Green Laser Powder Bed Fusion of Pure Copper in Combination with Chemical Post-Processing for RF Cavity Fabrication. *Instruments* **2024**, *8*, 39. [CrossRef]
108. Gradl, P.; Mireles, O.R.; Katsarelis, C.; Smith, T.M.; Sowards, J.; Park, A.; Chen, P.; Tinker, D.C.; Protz, C.; Teasley, T.; et al. Advancement of Extreme Environment Additively Manufactured Alloys for next Generation Space Propulsion Applications. *Acta Astronaut.* **2023**, *211*, 483–497. [CrossRef]
109. Gradl, P.R.; Protz, C.; Greene, S.E.; Ellis, D.; Lerch, B.; Locci, I. Development and Hot-Fire Testing of Additively Manufactured Copper Combustion Chambers for Liquid Rocket Engine Applications. In Proceedings of the 53rd AIAA/SAE/ASEE Joint Propulsion Conference, Atlanta, GA, USA, 10–12 July 2017.
110. Kerstens, F.; Cervone, A.; Gradl, P. End to End Process Evaluation for Additively Manufactured Liquid Rocket Engine Thrust Chambers. *Acta Astronaut.* **2021**, *182*, 454–465. [CrossRef]
111. Lu, P.; Shi, X.; Ye, X.; Wang, H.; Wu, M. Additive Manufactured High-Performance Topology-Optimized Lattice Structure: Compressive Behavior and Flow Heat Transfer Characteristics. *Case Stud. Therm. Eng.* **2024**, *61*, 105097. [CrossRef]
112. Sheykhpoor, H.; Darabkhani, H.G.; Awan, A.W. Improving Efficiency of Micro Gas Turbine Systems by Integration of Combustor and Recuperator Using Additive Manufacturing Techniques. *Int. J. Adv. Manuf. Technol.* **2023**, *127*, 23–44. [CrossRef]
113. Demir, A.G.; Colopi, M.; Previtali, B. The Use of a Ns-Pulsed, High Repetition Rate Green Laser for SLM of 99.9% Pure Cu. In Proceedings of the Lasers in Manufacturing Conference, Munich, Germany, 24–27 June 2019; pp. 1–8.